

1 **Large but decreasing effect of ozone on the European carbon**
2 **sink**

3 Rebecca J Oliver¹, Lina M Mercado^{1,2}, Stephen Sitch², David Simpson^{3,4}, Belinda E Medlyn⁵,
4 Yan-Shih Lin⁵, Gerd A Folberth⁶

5

6 ¹ Centre for Ecology and Hydrology, Benson Lane, Wallingford, OX10 8BB, UK

7 ² College of Life and Environmental Sciences, University of Exeter, EX4 4RJ, Exeter, UK

8 ³ EMEP MSC-W Norwegian Meteorological Institute, PB 43, NO-0313, Oslo, Norway

9 ⁴ Dept. Space, Earth & Environment, Chalmers University of Technology, Gothenburg, SE-41296 Sweden

10 ⁵ Hawkesbury Institute for the Environment, Western Sydney University, Locked Bag 1797, Penrith NSW 2751
11 Australia

12 ⁶ Met Office Hadley Centre, Exeter, UK.

13 *Correspondence to:* Rebecca Oliver (rfu@ceh.ac.uk)

14

15

16

17

18

19

20

21

22

23

24

25

26 **Abstract**

27

28 The capacity of the terrestrial biosphere to sequester carbon and mitigate climate change is governed by the ability
29 of vegetation to remove emissions of CO₂ through photosynthesis. Tropospheric O₃, a globally abundant and
30 potent greenhouse gas, is, however, known to damage plants, causing reductions in primary productivity. Despite
31 emission control policies across Europe, background concentrations of tropospheric O₃ have risen significantly
32 over the last decades due to hemispheric-scale increases in O₃ and its precursors. Therefore, plants are exposed to
33 increasing background concentrations, at levels currently causing chronic damage. Studying the impact of O₃ on
34 European vegetation at the regional scale is important for gaining greater understanding of the impact of O₃ on
35 the land carbon sink at large spatial scales. In this work we take a regional approach and update the JULES land-
36 surface model using new measurements specifically for European vegetation. Given the importance of stomatal
37 conductance in determining the flux of O₃ into plants, we implement an alternative stomatal closure
38 parameterization and account for diurnal variations in O₃ concentration in our simulations. We conduct our
39 analysis specifically for the European region to quantify the impact of tropospheric O₃, and its interaction with
40 CO₂, on gross primary productivity (GPP) and land carbon storage across Europe. A factorial set of model
41 experiments showed that tropospheric O₃ can suppress terrestrial carbon uptake across Europe over the period
42 1901 to 2050. By 2050, simulated GPP was reduced by 4 to 9% due to plant O₃ damage and land carbon storage
43 by 3 to 7%. The combined physiological effects of elevated future CO₂ (acting to reduce stomatal opening) and
44 reductions in O₃ concentrations resulted in reduced O₃ damage in the future. This alleviation of O₃ damage by
45 CO₂ induced stomatal closure was around 1 to 2% for low and high sensitivity respectively (on both land carbon
46 and GPP). Reduced land carbon storage resulted from diminished soil carbon stocks consistent with the reduction
47 in GPP. Regional variations are identified with larger impacts shown for temperate Europe (GPP reduced by 10
48 to 20%) compared to boreal regions (GPP reduced by 2 to 8%). These results highlight that O₃ damage needs to
49 be considered when predicting GPP and land carbon, and that the effects of O₃ on plant physiology need to be
50 considered in regional land carbon cycle assessments.

51

52

53

54

55

56

57

58

59 1 Introduction

60

61 The terrestrial biosphere absorbs around 30% of anthropogenic CO₂ emissions and acts to mitigate climate change
62 Le Quéré et al. (2015). Early estimates of the European carbon balance suggest a terrestrial carbon sink of between
63 135 to 205 TgC yr⁻¹ (Janssens et al., 2003). Schulze et al. (2009) determined a larger carbon sink of 274 TgC yr⁻¹,
64 and more recent estimates suggest a European terrestrial sink of between 146 to 184 TgC yr⁻¹ (Luysaert et al.,
65 2012). The carbon sink capacity of land ecosystems is dominated by the ability of vegetation to sequester carbon
66 through photosynthesis and release it back to the atmosphere through respiration. Therefore, any change in the
67 balance of these fluxes will alter ecosystem source-sink behaviour.

68

69 In recent decades much attention has focussed on the effects of rising atmospheric CO₂ on vegetation productivity
70 (Ceulemans and Mousseau, 1994;Norby et al., 2005;Norby et al., 1999;Saxe et al., 1998). The Norby et al. (2005)
71 synthesis of Free Air CO₂ Enrichment (FACE) experiments suggests a median stimulation (23 ± 2%) of forest
72 NPP in response to a doubling of CO₂. Similar average increases (20%) were observed for C₃ crops, although this
73 translated into smaller gains in biomass (17%) and crop yields (13%) (Long et al., 2006). Little attention, however,
74 has been given to tropospheric ozone (O₃), a globally abundant air pollutant recognised as one of the most
75 damaging pollutants for forests (Karlsson et al., 2007;Royal-Society, 2008;Simpson et al., 2014b). Tropospheric
76 O₃ is a secondary air pollutant formed by photochemical reactions involving carbon monoxide (CO), volatile
77 organic compounds (VOCs), methane (CH₄) and nitrogen oxides (NO_x) from both man-made and natural sources,
78 as well as downward transport from the stratosphere and lightning which is a source of NO_x. The phytotoxic
79 effects of O₃ exposure are shown to decrease vegetation productivity and biomass, with consequences for
80 terrestrial carbon sequestration (Felzer et al., 2004;Loya et al., 2003;Mills et al., 2011b;Sitch et al., 2007). Few
81 studies, however, consider the simultaneous effects of exposure to both gases, and few Earth-system models
82 (ESMs) currently explicitly consider the role of tropospheric O₃ in terrestrial carbon dynamics (IPCC, 2013), both
83 of which are important to understanding the carbon sequestration potential of the land-surface, and future carbon
84 dynamics regionally and globally (Le Quéré et al., 2016;Sitch et al., 2015).

85

86 Due to increased anthropogenic precursor emissions over the industrial period, background concentrations of
87 ground-level O₃ have risen (Vingarzan, 2004). O₃ levels at the start of the 20th century are estimated to be around
88 10 ppb for the site Montsouris Observatory near Paris, data for Arkona on the Baltic coast increased from ca. 15
89 ppb in the 1950s to 20-27 ppb by the early 1980s, and the Irish coast site Mace Head shows around 40 ppb by the
90 year 2000 (Logan et al., 2012;Parrish et al., 2012). Present day annual average background O₃ concentrations
91 reported in the review of Vingarzan (2004) show O₃ concentrations range between approximately 20 and 45 ppb,
92 with the greatest increase occurring since the 1950s. Trends vary from site to site though, even on a decadal basis
93 (Logan et al., 2012;Simpson et al., 2014b), depending, for example, on local/regional trends in precursor
94 (especially NO_x) emissions, elevation, and exposure to long-range transport. Nevertheless, there is some
95 indication that background O₃ levels over the mid-latitudes of the Northern Hemisphere have continued to rise at
96 a rate of approximately 0.5–2% per year, although not uniform (Vingarzan, 2004). As a result of controls on
97 precursor emissions in Europe and North America, peak O₃ concentrations in these regions have decreased or
98 stabilised over recent decades (Cooper et al., 2014;Logan et al., 2012;Parrish et al., 2012;Simpson et al., 2014b).

99 Nevertheless, climate change may increase the frequency of weather events conducive to peak O₃ incidents in the
100 future (e.g. summer droughts and heat-waves; e.g., (Sicard et al., 2013)), and may increase biogenic emissions of
101 the O₃-precursors isoprene and NO_x, although such impacts are subject to great uncertainty (Simpson et al.,
102 2014b;Young et al., 2013;Young et al., 2009). Intercontinental transport of air pollution from regions such as Asia
103 that currently have poor emission controls are thought to contribute substantially to rising background O₃
104 concentrations over the last decades (Cooper et al., 2010;Verstraeten et al., 2015). Northern Hemisphere
105 background concentrations of O₃ are now close to established levels for impacts on human health and the terrestrial
106 environment (Royal-Society, 2008). Therefore, although peak O₃ concentrations are in decline across Europe,
107 plants are exposed to increasing background levels, at levels currently causing chronic damage (Mills et al.,
108 2011b). Intercontinental transport means future O₃ concentrations in Europe will be partly dependent on how O₃
109 precursor emissions evolve globally.

110

111 Elevated O₃ concentrations impact agricultural yields and nutritional quality of major crops (Ainsworth et al.,
112 2012;Avnery et al., 2011), with consequences for global food security (Tai et al., 2014). As well as being a
113 significant air pollutant, O₃ is a potent greenhouse gas (Royal-Society, 2008). High levels of O₃ are damaging to
114 ecosystem health and reduce the global land carbon sink (Arneth et al., 2010;Sitch et al., 2007). Reduced uptake
115 of carbon by plant photosynthesis due to O₃ damage allows more CO₂ to remain in the atmosphere. This effect of
116 O₃ on plant physiology represents an additional climate warming to the direct radiative forcing of O₃ (Collins et
117 al., 2010;Sitch et al., 2007), the magnitude of which, however, remains highly uncertain (IPCC, 2013).

118

119 Dry deposition of O₃ to terrestrial surfaces, primarily uptake by stomata on plant foliage and deposition on external
120 surfaces of vegetation (Fowler et al., 2001;Fowler et al., 2009), is a large sink for ground level O₃ (Wild,
121 2007;Young et al., 2013). On entry to sub-stomatal spaces, O₃ reacts with other molecules to form reactive oxygen
122 species (ROS). Plants can tolerate a certain level of O₃ depending on their capacity to scavenge and detoxify the
123 ROS (Ainsworth et al., 2012). Above this critical level, long-term chronic O₃ exposure reduces plant
124 photosynthesis and biomass accumulation (Ainsworth, 2008;Ainsworth et al., 2012;Matyssek et al., 2010a;Wittig
125 et al., 2007;Wittig et al., 2009), either directly through effects on photosynthetic machinery such as reduced
126 Rubisco content (Ainsworth et al., 2012;Wittig et al., 2009) and/or indirectly by reduced stomatal conductance
127 (g_s) (Kitao et al., 2009;Wittig et al., 2007), alters carbon allocation to different pools (Grantz et al., 2006;Wittig
128 et al., 2009), accelerates leaf senescence (Ainsworth, 2008;Nunn et al., 2005;Wittig et al., 2009) and changes plant
129 susceptibility to biotic stress factors (Karnosky et al., 2002;Percy et al., 2002).

130

131 The response of plants to O₃ is very wide ranging as reported in the literature from different field studies. The
132 Wittig et al. (2007) meta-analysis of temperate and boreal tree species showed future concentrations of O₃
133 predicted for 2050 significantly reduced leaf level light saturated net photosynthetic uptake (-19%, range: -3% to
134 -28% at a mean O₃ concentration of 85 ppb) and g_s (-10%, range: +5% to -23% at a mean O₃ concentration of 91
135 ppb) in both broadleaf and needle leaf tree species. In the Feng et al. (2008) meta-analysis of wheat, projected O₃
136 concentrations for the future reduced aboveground biomass (-18% at a mean O₃ concentration of 70 ppb)
137 photosynthetic rate (-20% at a mean O₃ concentration of 73 ppb) and g_s (-22% at a mean O₃ concentration of 79
138 ppb). One of few long-term field based O₃ exposure studies (AspenFACE) showed that after 11 years of exposing

139 mature trees to elevated O₃ concentrations (mean O₃ concentration of 46 ppb), O₃ decreased ecosystem carbon
140 content (-9%), and decreased NPP (-10%), although the O₃ effect decreased through time (Talhelm et al., 2014).
141 Zak et al. (2011) showed this was partly due to a shift in community structure as O₃-tolerant species, competitively
142 inferior in low O₃ environments, out competed O₃-sensitive species. GPP was reduced (-12% to -19%) at two
143 Mediterranean ecosystems exposed to high ambient O₃ concentrations (ranging between 20 to 72 ppb across sites
144 and through the year) studied by Fares et al. (2013). Biomass of mature beech trees was reduced (-44%) after 8
145 years of exposure to elevated O₃ (~150 ppb) (Matyssek et al., 2010a). After 5 years of O₃ exposure (ambient +20
146 to +40 ppb) in a semi-natural grassland, annual biomass production was reduced (-23%), and in a Mediterranean
147 annual pasture O₃ exposure significantly reduced total aboveground biomass (up to -25%) (Calvete-Sogo et al.,
148 2014). However, these were empirical studies at individual sites, and these focus on O₃ effects on plant physiology
149 and productivity, but do not quantify the impact on the land carbon sink. Modelling studies are needed to scale
150 site observations to the regional and global scales. Models generally suggest that plant productivity and carbon
151 sequestration will decrease with O₃ pollution, though the magnitudes vary. For example, based on a limited dataset
152 to parameterise plant O₃ damage for a global set of plant functional types, Sitch et al. (2007) predicted a decline
153 in global GPP of 14 to 23% by 2100. A second study by Lombardozzi et al. (2015) similarly predicted a 10.8%
154 decrease of global GPP. Here we take a regional approach and take advantage of the latest measurements showing
155 changes in plant productivity with accumulated exposure to O₃ specifically for a range of European vegetation
156 from different regions (CLRTAP 2017) with which to calibrate the JULES model for plant sensitivity to O₃, and
157 conduct our analysis specifically for the European region.

158

159 Understanding the response of plants to elevated tropospheric O₃ is challenged by the large variation in O₃
160 sensitivity both within and between species (Karnosky et al., 2007; Kubiske et al., 2007; Wittig et al., 2009).
161 Additionally, other environmental stresses that affect stomatal behaviour will affect the rate of O₃ uptake and
162 therefore the response to O₃ exposure, such as high temperature, drought and changing concentrations of
163 atmospheric CO₂ (Mills et al., 2016; Fagnano et al., 2009; Kitao et al., 2009; Löw et al., 2006). Increasing
164 concentrations of atmospheric CO₂, for example, are suggested to provide some protection against O₃ damage by
165 causing stomata to close (Harmens et al., 2007; Wittig et al., 2007), however the long-term effects of CO₂
166 fertilisation on plant growth and carbon storage remain uncertain (Baig et al., 2015; Ciais et al., 2013). Further, in
167 some studies, stomata have been shown to respond sluggishly, losing their responsiveness to environmental
168 stimuli with exposure to O₃ which can lead to higher O₃ uptake, increased water-loss and therefore greater
169 vulnerability to environmental stresses such as drought (Mills et al., 2016; Mills et al., 2009; Paoletti and Grulke,
170 2010; Wilkinson and Davies, 2009).

171

172 Given the critical role g_s plays in the uptake of both CO₂ and O₃, we use an alternative representation and
173 parameterisation of g_s in JULES by implementing the Medlyn *et al.* (2011) g_s formulation. This model is based
174 on the optimal theory of stomatal behaviour and has advantages over the current JULES g_s formulation of Jacobs
175 (1994) including i) a single parameter (g_1) compared to two parameters in Jacobs (1994), ii) the g_1 parameter is
176 related to the water-use strategy of vegetation and is easier to parameterise with commonly measured leaf or
177 canopy level observations of photosynthesis, g_s and humidity, and (iii) values of g_1 are available for many
178 different plant functional types (PFTs) derived from a global data set of leaf-level measurements (Lin et al., 2015).

179

180 The main objective of this work is to assess the impact of historical and projected (1901 to 2050) changes in
181 tropospheric O₃ and atmospheric CO₂ concentration on predicted GPP and the land-carbon sink for Europe.
182 These are the two greenhouse gases that directly affect plant photosynthesis and g_s . We use a factorial suite of
183 model experiments, using the Joint UK land environment simulator (JULES) (Best et al., 2011; Clark et al.,
184 2011), the land-surface model of the UK Earth System Model (UKESM) (Collins et al., 2011) to simulate plant
185 O₃ uptake and damage, and to investigate the impact of both O₃ and CO₂ on plant water-use and carbon uptake.
186 In this work, the JULES model is re-calibrated using the latest observations of vegetation sensitivity to O₃, with
187 the addition of a separate parameterisation for temperate/boreal regions versus the Mediterranean. The O₃
188 sensitivity of each PFT in JULES was re-calibrated for both a high and low sensitivity to account for uncertainty
189 in the O₃ response, in part due to the observed variation in O₃ sensitivity between species. This includes O₃
190 sensitivities for agricultural crops (wheat – high sensitivity) versus natural grassland (low sensitivity), with
191 separate sensitivities for Mediterranean grasslands. For forests JULES is parameterised with O₃ sensitivities for
192 broadleaf and needle leaf trees (with a high and low O₃ sensitivity for both), with separate sensitivities (high and
193 low) for Mediterranean broadleaf species. We make a separate distinction for the Mediterranean region where
194 possible because the work of Büker et al. (2015) showed that different O₃ dose-response relationships are
195 needed to describe the O₃ sensitivity of dominant Mediterranean trees. In addition, we introduce an alternative g_s
196 scheme into JULES as described above. JULES is forced with spatially varying daily O₃ concentrations from a
197 high resolution atmospheric chemistry model for Europe that are disaggregated to hourly concentrations,
198 therefore our simulations account for diurnal variations in O₃ concentration and O₃ responses allowing for
199 improved estimates of O₃ uptake by vegetation. We do not attempt to make a full assessment of the carbon cycle
200 of Europe, instead we target O₃ damage, which is currently a missing component in earlier carbon cycle
201 assessments (Le Quéré et al., 2017; Sitch et al., 2015). To this end, we prescribe changing O₃ and CO₂
202 concentrations from 1901 to 2050, but use a fixed pre-industrial climate. We acknowledge the use of a 'fixed'
203 pre-industrial climate omits the additional uncertainty of the interaction between climate change and g_s which
204 will affect the rate of O₃ uptake and therefore O₃ concentrations. In addition, using uncoupled chemistry and
205 climate is a further source of uncertainty. To understand the impact of these complex feedback mechanisms is
206 an important area for future work, but in the current study our aim is to isolate the physiological response of
207 plants to both O₃ and CO₂, and determine the sensitivity of predicted GPP and the land carbon sink to this
208 process, as the impact of O₃ on the land carbon sink currently remains largely unknown at large spatial scales
209 for Europe.

210

211

212

213 **2 Methods**

214

215 **2.1 Representation of O₃ effects in JULES**

216

217 JULES calculates the land-atmosphere exchanges of heat, energy, mass, momentum and carbon on a sub-daily
218 time step, and includes a dynamic vegetation model (Best et al., 2011; Clark et al., 2011; Cox, 2001). This work

219 uses JULES version 3.3 (<http://www.jchmr.org>) at 0.5° x 0.5° spatial resolution and hourly model time step, the
 220 spatial domain is shown in Fig. S5. JULES has a multi-layer canopy radiation interception and photosynthesis
 221 scheme (10 layers in this instance) that accounts for direct and diffuse radiation, sun fleck penetration through the
 222 canopy, inhibition of leaf respiration in the light and change in photosynthetic capacity with depth into the canopy
 223 (Clark et al., 2011; Mercado et al., 2009). Soil water content also affects the rate of photosynthesis and g_s . It is
 224 modelled using a dimensionless soil water stress factor, β , which is related to the mean soil water concentration
 225 in the root zone, and the soil water contents at the critical and wilting point (Best *et al.*, 2011).

226

227 To simulate the effects of O₃ deposition on vegetation productivity and water use, JULES uses the flux-gradient
 228 approach of Sitch *et al.*, (2007), modified to include non-stomatal deposition following Tuovinen et al. (2009). A
 229 similar approach is taken by Franz et al. (2017) in the OCN model, however plant O₃ damage is a function of
 230 accumulated O₃ exposure over time. In JULES, plant O₃ damage is instantaneous, the degree to which
 231 photosynthesis and g_s are modified at each time step with O₃ exposure having already been calibrated against
 232 observations of the change in plant productivity with cumulative O₃ exposure for each PFT (i.e. O₃ dose-response
 233 functions described later). JULES uses a coupled model of g_s and photosynthesis, the potential net photosynthetic
 234 rate (A_p , mol CO₂ m⁻² s⁻¹) is modified by an 'O₃ uptake' factor (F , the fractional reduction in photosynthesis), so
 235 that the actual net photosynthesis (A_{net} , mol CO₂ m⁻² s⁻¹) is given by equation 1 (Clark *et al.*, 2011, Sitch *et al.*,
 236 2007). Because of the relationship between these two fluxes, the direct effect of O₃ damage on photosynthetic rate
 237 also leads to a reduction in g_s . An alternative approach was taken by Lombardozzi et al. (2012) in the CLM model
 238 where photosynthesis and g_s are decoupled, so that O₃ exposure affects carbon assimilation and transpiration
 239 independently. In JULES, changes in atmospheric CO₂ concentration also affect photosynthetic rate and g_s ,
 240 consequently the interaction between changing concentrations of both CO₂ and O₃ is allowed for.

241

$$242 \quad A_{net} = A_p F \quad (1)$$

243

244 The O₃ uptake factor (F) is defined as:

245

$$246 \quad F = 1 - a * \max[F_{O_3} - F_{O_3crit}, 0.0] \quad (2)$$

247

248 F_{O_3} is the instantaneous leaf uptake of O₃ (nmol m⁻² s⁻¹), F_{O_3crit} is a PFT-specific threshold for O₃ damage (nmol
 249 m⁻² PLA s⁻¹, projected leaf area), and 'a' is a PFT-specific parameter representing the fractional reduction of
 250 photosynthesis with O₃ uptake by leaves. Following Tuovinen et al. (2009), the flux of O₃ through stomata, F_{O_3} ,
 251 is represented as follows:

252

$$253 \quad F_{O_3} = O_3 \left(\frac{g_b \left(\frac{g_l}{K_{O_3}} \right)}{g_b + \left(\frac{g_l}{K_{O_3}} \right) + g_{ext}} \right) \quad (3a)$$

254

255 O_3 is the molar concentration of O₃ at reference (canopy) level (nmol m⁻³), g_b is the leaf-scale boundary layer
 256 conductance (m s⁻¹, eq 3b), g_l is the leaf conductance for water (m s⁻¹), K_{O_3} accounts for the different diffusivity of
 257 ozone to water vapour and takes a value of 1.51 after Massman (1998), and g_{ext} is the leaf-scale non-stomatal

258 deposition to external plant surfaces (m s^{-1}) which takes a constant value of 0.0004 m s^{-1} after Tuovinen et al.
259 (2009). The leaf-level boundary layer conductance (g_b) is calculated as in Tuovinen *et al.* (2009)

260

$$261 \quad g_b = \alpha Ld^{-1/2} U^{-1/2} \quad (3b)$$

262

263 α is a constant ($0.0051 \text{ m s}^{-1/2}$), Ld is the cross-wind leaf dimension (m) defined per PFT as 0.05 for trees, 0.02
264 for grasses (C_3 and C_4) and 0.04 for shrubs, U is wind speed at canopy height (m s^{-1}). The rate of O_3 uptake is
265 dependent on g_s , which is dependent on photosynthetic rate. Given g_s is a linear function of photosynthetic rate in
266 JULES (Clark et al., 2011), from eq 1 it follows that:

267

$$268 \quad g_s = g_l F \quad (4)$$

269

270 The O_3 flux to stomata, F_{O_3} , is calculated at leaf level and then scaled to each canopy layer differentiating sunlit
271 and shaded leaf photosynthesis, and finally summed up to the canopy level. Because the photosynthetic capacity,
272 photosynthesis and therefore g_s decline with depth into the canopy, this in turn affects O_3 uptake, with the top leaf
273 level contributing most to the total O_3 flux and the lowest level contributing least.

274

275 **2.2 Calibration of O_3 uptake model**

276

277 Here we use the latest literature on flux based O_3 dose-response relationships derived from observed field data
278 across Europe (CLRTAP, 2017) to determine the key PFT-specific O_3 sensitivity parameters in JULES (a and
279 $F_{\text{O}_3\text{crit}}$). Synthesis of information expressed as O_3 flux based dose-response relationships derived from field
280 experiments is carried out by The United Nations Convention on Long-Range Transboundary Air Pollution
281 (CLRTAP Convention), this information is then used as a policy tool to inform emission reduction strategies in
282 Europe to improve air quality (CLRTAP, 2017; Mills et al., 2011a). Derivation of O_3 flux based dose-response
283 relationships for different vegetation types uses the accumulated stomatal O_3 flux above a threshold (often referred
284 to as the phytotoxic O_3 dose above a threshold of 'y' i.e. POD_y) as the dose metric, and the percentage change in
285 biomass as the response metric (Emberson et al., 2007; Karlsson et al., 2007). We use these observation based O_3
286 dose-response relationships to calibrate each JULES PFT for sensitivity to O_3 using available relationships for the
287 closest matching vegetation type. For JULES, $F_{\text{O}_3\text{crit}}$ is the threshold for O_3 damage, and values for this parameter
288 are taken from the O_3 dose-response relationships as the POD_y value. The actual sensitivity to O_3 is determined
289 by the slope of the O_3 dose-response relationship, i.e. how much biomass changes with accumulated stomatal
290 uptake of O_3 above the damage threshold, this relates to the parameter a in JULES. The parameter ' a ' is a PFT-
291 specific parameter representing the fractional reduction of photosynthesis with O_3 uptake by leaves. Values for
292 this parameter are found for each PFT by running JULES with different values of ' a ', which alter the instantaneous
293 photosynthetic rate, but then calculating the accumulated stomatal flux of O_3 and the change in productivity, until
294 the slope of this relationship produced by the JULES simulations matches that of the O_3 dose-response
295 relationships derived from observations. Essentially we calibrate each JULES PFT for sensitivity to O_3 by
296 reproducing the observation-based O_3 dose-response relationships.

297

298 Each PFT was calibrated for a high and low plant O₃ sensitivity to account for uncertainty in the sensitivity of
299 different plant species to O₃, using the approach of Sitch *et al.*, (2007). Therefore, when using our results to assess
300 the impact of O₃ at the land surface, we are able to provide a range in our estimates to help address some of the
301 uncertainty in the O₃ response of different vegetation types. In addition, where possible owing to available data,
302 a distinction was made for Mediterranean regions. This was because the work of B ker et al. (2015) showed that
303 different O₃ dose-response relationships are needed to describe the O₃ sensitivity of dominant Mediterranean trees.
304 For the C₃ herbaceous PFT, the dominant land cover type across the European domain in this study (Fig. S1), the
305 high plant O₃ sensitivity was calibrated against observations for wheat to give a representation of agricultural
306 regions and wheat is one of the most sensitive grasses to O₃ (Fig. S2, Table S1). For the low plant O₃ sensitivity
307 JULES was calibrated against the dose-response function for natural grassland to give a representation of natural
308 grassland and this vegetation has a much lower sensitivity to O₃ damage, for the Mediterranean region we used a
309 function for Mediterranean natural grasslands, all taken from CLRTAP (2017) (Fig. S2, Table S1). Tree/shrub
310 PFTs were calibrated against observed O₃ dose-response functions for the high plant O₃ sensitivity: broadleaf
311 trees (temperate/boreal) = Birch/Beech dose-response relationship, broadleaf trees (Mediterranean) = deciduous
312 oaks dose-response relationship, needle leaf trees = Norway spruce dose-response relationship, shrubs =
313 Birch/Beech dose-response relationship, all from CLRTAP (2017) (Fig. S2, Table S1). Data on O₃ dose-response
314 relationships for different vegetation types is very limited, therefore for the low plant O₃ sensitivity calibration for
315 trees/shrubs we assumed a 20% decrease in sensitivity to O₃ based on the difference in sensitivity between high
316 and low sensitive tree species in the Karlsson et al. (2007) study. Due to limitations in data availability, the shrub
317 parameterisation uses the observed dose-response functions for broadleaf trees. Similarly, the parameterisation
318 for C₄ herbaceous uses the observed dose-responses for C₃ herbaceous, however the fractional cover of C₄ herbs
319 across Europe is low (Fig. S1), so this assumption affects a very small percentage of land cover.

320

321 To calibrate the JULES O₃ uptake model, JULES was run across Europe forced using the WFDEI observational
322 climate dataset (Weedon, 2013) at 0.5° X 0.5° spatial and three hour temporal resolution. JULES uses interpolation
323 to disaggregate the forcing data down from 3 hours to an hourly model time step. The model was spun-up over
324 the period 1979 to 1999 with a fixed atmospheric CO₂ concentration of 368.33 ppm (1999 value from Mauna Loa
325 observations, (Tans and Keeling)). Zero tropospheric ozone concentration was assumed for the control simulation,
326 for the simulations with O₃, spin-up used spatially explicit fields of present day O₃ concentration produced using
327 the UK Chemistry and Aerosol (UKCA) model with standard chemistry from the run evaluated by O'Connor et
328 al. (2014). A fixed land cover map was used based on IGBP (International Geosphere-Biosphere Programme)
329 land cover classes (IGBP-DIS), therefore as the vegetation distribution was fixed and the calibration was not
330 looking at carbon stores, a short spin-up was adequate to equilibrate soil temperature and soil moisture. JULES
331 was then run for the year 2000 with a corresponding CO₂ concentration of 369.52 ppm (from Mauna Loa
332 observations, (Tans and Keeling)) and monthly fields of spatially explicit tropospheric O₃ (O'Connor et al., 2014)
333 as necessary.

334

335 Calibration was performed using four simulations: with i) zero tropospheric O₃ concentration, this was the control
336 simulation (control), ii) tropospheric O₃ at current ambient concentration (O₃), iii) ambient +20 ppb (O₃+20) and
337 iv) ambient +40 ppb (O₃+40). The different O₃ simulations (i.e. O₃, O₃+20 and O₃+40) were used to capture the

338 range of O₃ conditions in the data used in the observation-based O₃ dose-response relationships used in this study
339 for calibration, often data were from experiments using artificially manipulated conditions of ambient + 40 ppb
340 O₃ for example. For each JULES O₃ simulation, the value of F_{O_3crit} was taken from the vegetation specific O₃
341 dose-response relationship as the threshold O₃ concentration above which damage to vegetation occurs. An initial
342 estimate of the parameter ‘ a ’ was used, then for each PFT and each simulation, hourly estimates of NPP (our
343 proxy for biomass – although not identical they are related) and O₃ uptake in excess of F_{O_3crit} were accumulated
344 over a PFT dependent accumulation period. The accumulation periods were ~6 months for broadleaf trees and
345 shrubs, all year for needle leaf trees, and ~3 months for herbaceous species, through the growing season, following
346 guidelines in CLRTAP (2017). Additionally, in accordance with the methods used in the CLRTAP (2017) that
347 describe how the O₃ dose-response relationships are derived from observations, we use the stomatal O₃ flux per
348 projected leaf area to top canopy sunlit leaves. The percentage change in total NPP was calculated for each O₃
349 simulation and plotted against the cumulative uptake of O₃ over the PFT-specific accumulation period. The linear
350 regression of this relationship was calculated, and slope and intercept compared against the slope and intercept of
351 the observed dose-response relationships. Values of the parameter ‘ a ’ were adjusted, and the procedure repeated
352 until the linear regression through the simulation points matched that of the observations (Fig. S2, Table S1).

353

354 2.3 Representation of stomatal conductance and site level evaluation

355

356 In JULES, g_s (m s⁻¹) is represented following the closure proposed by (Jacobs, 1994):

357

$$358 \quad g_s = 1.6RT_l \frac{A_{net}\beta}{c_a - c_i} \quad (5)$$

359

360 In this parameterisation, c_i is unknown and in the default JULES model is calculated as in equation 6, hereafter
361 called JAC:

362

$$363 \quad c_i = (c_a - c_*)f_0 \left(1 - \frac{dq}{dq_{crit}}\right) + c_* \quad (6)$$

364

365 β is a soil moisture stress factor, the factor 1.6 accounts for g_s being the conductance for water vapour rather than
366 CO₂, R is the universal gas constant (J K⁻¹ mol⁻¹), T_l is the leaf surface temperature (K), c_a and c_i (both Pa) are the
367 leaf surface and internal CO₂ partial pressures, respectively, c_* (Pa) is the CO₂ photorespiration compensation
368 point, dq is the humidity deficit at the leaf surface (kg kg⁻¹), dq_{crit} (kg kg⁻¹) and f_0 are PFT specific parameters
369 representing the critical humidity deficit at the leaf surface, and the leaf internal to atmospheric CO₂ ratio (c_i/c_a)
370 at the leaf specific humidity deficit (Best *et al.* 2011), values are shown in Table S1.

371

372 In this work, we replace equation 6 with the closure described in Medlyn *et al.* (2011), using the key PFT specific
373 model parameter g_l (kPa^{0.5}), and dq is expressed in kPa, shown in eq 7, hereafter called MED:

374

$$375 \quad c_i = c_a \left(\frac{g_l}{g_l + \sqrt{dq}} \right) \quad (7)$$

376

377 PFT specific values of the g_l parameter were derived for European vegetation from the data base of Lin et al.
378 (2015) and are shown in Table S1. The g_l parameter represents the sensitivity of g_s to the assimilation rate, i.e.
379 plant water use efficiency, and was derived as in Lin et al. (2015) by fitting the Medlyn *et al.*, (2011) model to
380 observations of g_s , photosynthesis, and VPD, with no g_0 term.

381

382 The impact of g_s model formulation (JAC versus MED) on simulated water, O_3 , carbon and energy fluxes is
383 compared for two contrasting grid points - wet (low soil moisture stress) and dry (high soil moisture stress) in the
384 European domain. JULES was spun-up for 20 years (1979-1999) at two grid points in central Europe representing
385 a wet (low soil moisture stress, lat: 48.25; lon.: 5.25) and a dry site (high soil moisture stress, lat: 38.25; lon.: -
386 7.75). The modelled soil moisture stress factor ($fsmc$) at the wet site ranged from 0.8 to 1.0 over the year 2000
387 (1.0 indicates no soil moisture stress), and at the dry site $fsmc$ steadily declined from 0.8 at the start of the year to
388 0.25 by the end of the summer. The WFDEI meteorological forcing dataset was used (Weedon, 2013), along with
389 atmospheric CO_2 concentration for the year 1999 (368.33 ppm), and either no O_3 (i.e. the O_3 damage model was
390 switched off) for the control simulations, or spatially explicit fields of present day O_3 concentration produced
391 using the UK Chemistry and Aerosol (UKCA) model from the run evaluated by O'Connor et al. (2014) for the
392 simulations with O_3 . Following the spin-up period, JULES was run for one year (2000) with corresponding
393 atmospheric CO_2 concentration, and tropospheric O_3 concentrations as described above. The control and O_3
394 simulations were performed for both JAC and MED model formulations. Land cover for the spin-up and main run
395 was fixed at 20% for each PFT. For the simulations including O_3 damage, the high plant O_3 sensitivity
396 parameterisation was used. The difference between these simulations was used to assess the impact of g_s model
397 formulation on the leaf level fluxes of carbon and water. We calculate and report (results section 3.1) the difference
398 in mean annual water-use that results from the above simulations using the different g_s models. For each day of
399 the simulation we calculate the percentage difference in water-use between the two simulations, we then calculate
400 the mean and standard deviation over the year to give the annual mean leaf-level water-use.

401

402 Site level evaluation of the two g_s models compared to FLUXNET observations was carried out to evaluate the
403 seasonal cycles of latent and sensible heat using the two g_s models JAC and MED compared to observations.
404 Seven Fluxnet towers were selected to represent a range of land cover types as shown in Table S2. JULES was
405 setup for each site using observed site-level hourly meteorology, and the vegetation cover was prescribed
406 according to the fractional covers of the different JULES surface types shown in Table S2. Following a spin-up
407 period, simulations were run at each site for the years shown in Table S2.

408

409 **2.4 Model simulations for Europe**

410

411 **2.4.1 Forcing datasets**

412

413 We used the WATCH meteorological forcing data set (Weedon et al., 2010; Weedon et al., 2011) at $0.5^\circ \times 0.5^\circ$
414 spatial and three hour temporal resolution for our JULES simulations. JULES interpolates this down to an hourly

415 model time step. For this study, the climate was kept constant by recycling over the period 1901 to 1920, to allow
416 us to focus on the impact O₃, CO₂ and their interaction.

417

418 JULES was run with prescribed annual mean atmospheric CO₂ concentrations. Pre-industrial global CO₂
419 concentrations (1900 to 1960) were taken from Etheridge et al. (1996), 1960 to 2002 were from Mauna Loa
420 (Keeling and Whorf, 2004), as calculated by the Global Carbon Project (Le Quéré et al., 2016), and 2003-2050
421 were based on the IPCC SRES A1B scenario and were linearly interpolated to gap fill missing years (Fig. 1).

422

423 JULES was run including dynamic vegetation with a land cover mask giving the fraction of agriculture in each
424 0.5° x 0.5° grid cell based on the Hurtt et al. (2011) land cover database for the year 2000. This means that whilst
425 the model is allowed to evolve its own vegetation cover, within the agricultural mask only C₃/C₄ herbaceous PFTs
426 are allowed to grow, with no competition from other PFTs. Therefore, through the simulation period, regions of
427 agriculture are maintained as such and not out-competed by forests for example, allowing for a more accurate
428 representation of the land cover of Europe in the model. No form of land management is simulated (i.e. no crop
429 harvesting, ploughing, rotation or grazing), growth and leaf area index (LAI) are determined by resource
430 availability and phenology. Outside of the agricultural mask, dynamic vegetation means that grid cell PFT
431 coverage and LAI are the result of resource availability, phenology and simulated competition. Across the model
432 domain, simulated mean annual LAI was dominantly within the range of 2 to 5 m²/m² (Fig. S3 and S4). Following
433 a full spin-up period (to ensure equilibrium vegetation, carbon and water states), there was no significant change
434 in the fractional cover of each PFT over the simulation period (1901 - 2050). By 2050, increases in boreal forest
435 cover occurred, but this was less than 2% and limited to very small areas, given this small change we show just
436 the land cover for 2050 in Fig. S1.

437

438 Tropospheric O₃ concentration was produced by the EMEP MSC-W model at 0.5° x 0.5° (Simpson et al., 2012),
439 driven with meteorology from the regional climate model RCA3 (Kjellström et al., 2011; Samuelsson et al., 2011),
440 which provides a downscaling of the ECHAM A1B-r3 (simulation 11 of Kjellström *et al.*, 2011). This setup
441 (EMEP+RCA3) is also used by Langner et al. (2012a), Simpson et al. (2014a), Tuovinen et al. (2013), Franz et
442 al. (2017) and Engardt et al. (2017), where further details and model evaluation can be found. Unfortunately, the
443 3-dimensional RCA3 data needed by the EMEP model was not available prior to 1960, but as in Engardt et al.
444 (2017) the meteorology of 1900-1959 had to be approximated by assigning random years from 1960 to 1969. This
445 procedure introduces some uncertainty of course, although Langner et al. (2012b) show that for the period 1990
446 to 2100 it is emissions change, rather than meteorological change, that drives modelled O₃ concentrations. The
447 emissions scenarios for 1900-2050 merge data from the International Institute of Applied System Analysis
448 (IIASA) for 2005-2050 (the so-called ECLIPSE 4a scenario), recently revised EMEP data for 1990, and a scaling
449 back from 1990 to 1900 using data from Lamarque et al. (2013). The trend in emissions of the major O₃ precursors
450 NO_x, NMVOC and Isoprene are shown from 1900 to 2050 over Europe in Fig. S5. Isoprene emissions are not
451 inputs to the EMEP model, but rather calculated at each time-step using temperature, radiation, and land-cover
452 specific emission factors (Simpson et al., 2012). Changes in the assumed background concentration of CH₄ (from
453 RCP6.0) (van Vuuren et al., 2011) are also shown in Fig. S5. Engardt et al. (2017) show the trend in emissions of

454 SO₂ and NH₃ from 1900 to 2050 over Europe. The EMEP model accounts for changes in BVOC emissions as a
455 result of predicted ambient temperature changes.

456

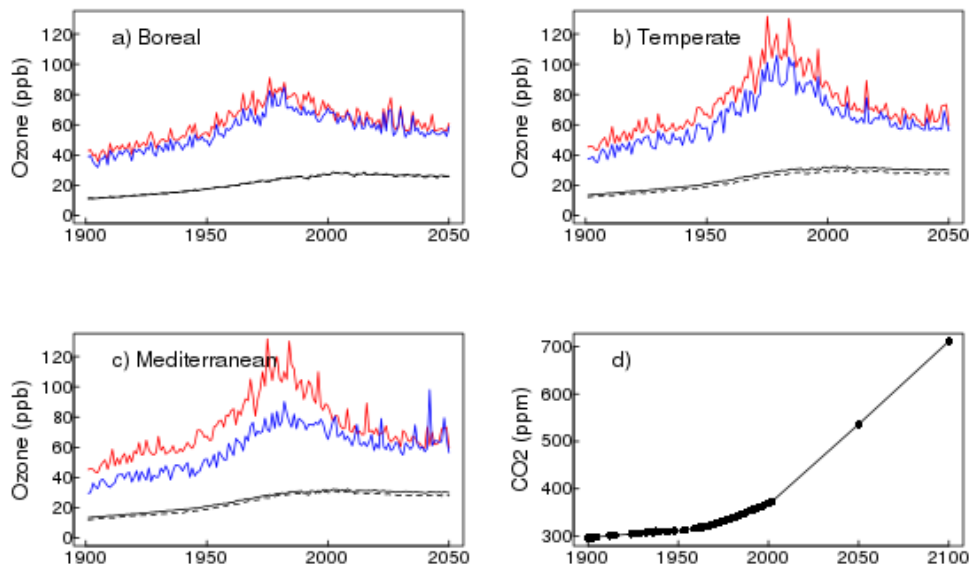
457 O₃ concentrations from EMEP MSC-W were calculated at canopy height for two land-cover categories: forest
458 and grassland (Fig. S6 and Fig. S7), which are taken as surrogates for high and low vegetation, respectively. These
459 canopy-height specific concentrations allow for the large gradients in O₃ concentration that can occur in the lowest
460 10s of metres, giving lower O₃ for grasslands than seen at e.g. 20 m in a forest canopy (Gerosa et al., 2017; Simpson
461 et al., 2012; Tuovinen et al., 2009). These canopy level O₃ concentrations are used as input to JULES, using the
462 EMEP O₃ concentrations for forest for the forest JULES PFTs (broadleaf/needle leaf tree and shrub), and the
463 EMEP O₃ concentrations for grassland for the grass/herbaceous JULES PFTs (C₃ and C₄). This study used daily
464 mean values of tropospheric O₃ concentration from EMEP disaggregated down to the hourly JULES model time-
465 step. The daily mean O₃ forcing was disaggregated to follow a mean diurnal profile of O₃, this was generated from
466 hourly O₃ output from EMEP MSC-W for the two land cover categories (forest and grassland as described above)
467 across the same model domain. O₃ concentrations follow a diurnal cycle and peak during the day, therefore
468 accounting for the diurnal variation in O₃ concentrations allows for a more realistic estimation of O₃ uptake.

469

470 Figure 1 shows large increases in tropospheric O₃ from pre-industrial to present day (2001), this is in line with
471 modelling studies (Young et al., 2013) and site observations (Derwent et al., 2008; Logan et al., 2012; Parrish et
472 al., 2012), and is predominantly a result of increasing anthropogenic emissions (Young et al., 2013). Figures S6
473 and S7 show this large increase in ground-level O₃ concentrations from 1901 to 2001 occurs in all seasons. Present
474 day O₃ concentration show a strong seasonal cycle, with a spring/summer peak in concentrations in the mid-
475 latitudes of the Northern Hemisphere (Derwent et al., 2008; Parrish et al., 2012; Vingarzan, 2004). Seasonal cycles
476 have been changing over the past decades however, attributed to changes in NO_x and other emissions, as well as
477 changes in transport patterns (Parrish et al., 2013). These changes will likely continue in future as emissions and
478 meteorological factors impact photo-chemical O₃ production and transport patterns. Indeed, the O₃ concentrations
479 used in the simulations in this study show increased O₃ levels in winter and in some regions in autumn and spring
480 in 2050 compared to present day, this may be due to reduced titration of O₃ by NO as a result of reduced NO_x
481 emissions in the future (Royal Society, 2008). Summer O₃ concentrations are lower in 2050 however, compared
482 to 2001.

483

484



485

486 **Figure 1.** Regional time series of canopy height O₃ (ppb) forcing from EMEP a) to c), and d) global atmospheric
 487 CO₂ (ppm) concentration (this does not vary regionally; black dots show data points, the black line shows
 488 interpolated points). Each panel for the O₃ forcing shows the regional annual average (woody PFTs, black solid
 489 line; herbaceous PFTs, black dashed line) and the annual maximum O₃ concentration above: woody PFTs (red)
 490 and herbaceous PFTs (blue).

491

492 2.4.2 Spin up and factorial experiments

493

494 JULES was spun-up by recycling the climate from the early part of the twentieth century (1901 to 1920) using
 495 atmospheric CO₂ (296.1 ppm) and O₃ concentrations from 1901 (Fig. S3 & Fig. S4). Model spin-up was 2000
 496 years by which point the carbon pools and fluxes were in steady state with zero mean net land – atmosphere CO₂
 497 flux. We performed the following transient simulations for the period 1901 to 2050 with continued recycling of
 498 the climate as used in the spin-up, for both high and low plant O₃ sensitivities:

499

- 500 • **O3** : Fixed 1901 CO₂, Varying O₃
- 501 • **CO2** : Varying CO₂, Fixed 1901 O₃
- 502 • **CO2+O3** : Varying CO₂, Varying O₃

503

504 We use these simulations to investigate the direct effects of changing atmospheric CO₂ and O₃ concentrations,
 505 individually and combined, on plant water-use, GPP and the land C sink through the twentieth century and into
 506 the future, specifically over three time periods: historical (1901-2001), future (2001-2050) and over the full time
 507 series (1901-2050). For each time period we calculate the difference between the decadal means calculated at the
 508 start and end of the analysis period for each variable of interest. Therefore our results report the change in GPP,
 509 for example, over the analysis period. For each variable analysed (GPP, NPP, vegetation carbon, soil carbon, total
 510 land carbon and *g_s*), we use the mean over 10 years to represent each time period, e.g. the mean over 2040 to 2050
 511 is what we call 2050, 1901 to 1910 is what we refer to as 1901. The difference between the simulations gives the
 512 effect of O₃ and CO₂ either separately or in combination over the different time periods. We look at the percentage

513 change due to either O₃ at pre-industrial CO₂ concentration (i.e. without the additional effect of atmospheric CO₂
514 on stomatal behaviour - O₃ simulation), CO₂ (at fixed pre-industrial O₃ concentration, CO₂ simulation) or the
515 combined effect of both gases (CO₂+O₃ simulation), which is calculated as:

516

$$517 \quad 100 * (\text{var}[y_1] - \text{var}[y_2]) / \text{var}[y_2] \quad (8)$$

518

519 Where var[y_x] represents the variable in time period y, e.g. 100 * (varO₃[2050] – varO₃[1901]) / varO₃[1901]
520 gives the O₃ effect (at fixed CO₂) over the full experimental period. The meteorological forcing is prescribed in
521 these simulations and is therefore the same between the model runs. Other climate factors, such as VPD,
522 temperature and soil moisture availability are accounted for in our simulations, but our analysis isolates the effects
523 of O₃, CO₂ and O₃ + CO₂. We also use paired t-test to determine statistically significant differences between the
524 different (high and low) plant O₃ sensitivities.

525

526 **2.4.3 Evaluation**

527 To evaluate our JULES simulations we compare mean GPP from 1991 to 2001 for each of the JULES scenarios
528 and both high and low plant O₃ sensitivities against the observation based globally extrapolated Flux Network
529 model tree ensemble (MTE) (Jung et al., 2011). We use paired t-test to determine statistically significant
530 differences in the mean responses.

531

532 **3 Results**

533

534 **3.1 Impact of g_s model formulation and site level evaluation**

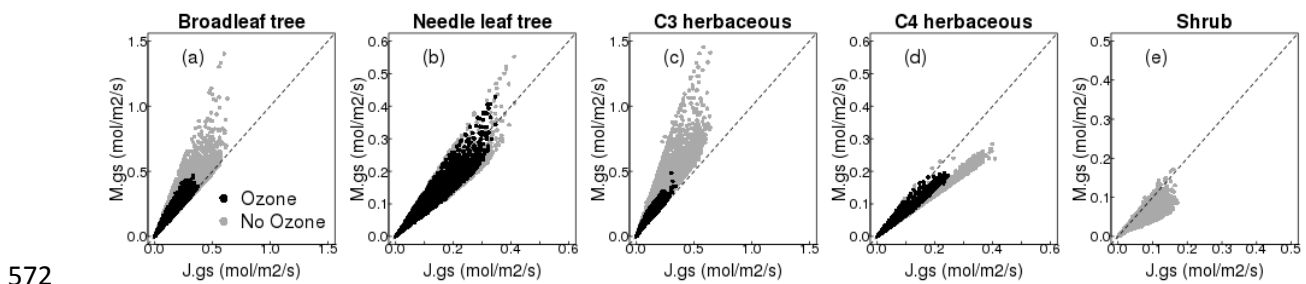
535

536 The impact of g_s model on simulated g_s is shown for the site with low soil moisture stress (wet site, Fig. 2). For
537 the broadleaf tree and C₃ herbaceous PFT, the MED model simulates a larger conductance compared to the JAC
538 model. In other words, with the MED model these two PFTs are parameterised with a less conservative water use
539 strategy, which, for the grid point shown in Fig. 2, increased the annual mean water use by 35% (±29%) and 45%
540 (±32%), respectively. In contrast, the needle leaf tree, C₄ herbaceous and shrub PFTs are parameterised with a
541 more conservative water use strategy with the MED model, and the mean annual g_s was decreased by 13% (±12%),
542 27% (±10%) and 36% (±13%), respectively, compared to the JAC model. This comparison was also done for a
543 dry site (high soil moisture stress), and similar results were found (Fig. S8). The effect of g_s formulation on
544 simulated photosynthesis was much smaller because of the lower sensitivity of the limiting rates of photosynthesis
545 to changes in c_i in the model compared to the effect of the same change in c_i on modelled g_s (Fig. S9 & S10).
546 Changes in g_s impact the partitioning of simulated energy fluxes. In general, increased g_s results in increased latent
547 heat and thus decreased sensible heat flux, and vice versa where g_s is decreased (Fig. S9 & S10). Also shown is
548 the effect of the MED model on O₃ flux into the leaf (Fig. S11 and Fig. S8 bottom panel). For the broadleaf tree
549 and C₃ herbaceous PFT, the MED model simulates a larger conductance and therefore a greater flux of O₃ through

550 stomata compared to JAC, and this is indicative of the potential for greater reductions in photosynthesis (Fig. S9
551 & S10 top row). The reverse is seen for the needle leaf tree, C₄ herbaceous and shrub PFTs.

552

553 Site level evaluation of the seasonal cycles of latent and sensible heat with both JAC and MED models compared
554 to FLUXNET observations showed in general, the MED model improved the seasonal cycle of both fluxes (lower
555 RMSE), but the magnitude of this varied from site to site (Fig. S12). At the deciduous broadleaf site, US-UMB,
556 MED resulted in improvements of the simulated seasonal cycle particularly in the summer months for both fluxes
557 (RMSE decreased from 42.7/31.5 to 38.5/28.0 W/m² for latent/sensible heat respectively). At the second
558 deciduous broadleaf site IT-CA1 however, there was almost no difference between the two g_s models. Both
559 evergreen needle leaf forest sites (FI-Hyy and DE-Tha) saw improvements in the simulated seasonal cycles of
560 latent and sensible heat with the MED model, primarily as a result of lower latent heat flux in the spring and
561 summer months, and higher sensible heat flux over the same period. At FI-Hyy, RMSE decreased from 10.1/7.4
562 to 6.7/6.7 W/m² for latent/sensible heat respectively, and at DE-Tha, RMSE decreased from 16.0/11.9 to 10.5/10.6
563 W/m² for latent/sensible heat respectively. With the MED model the monthly mean latent heat flux was improved
564 at the C₃ grass site (CH-Cha) as a result of increased flux in the summer months (RMSE decreased from 15.7 to
565 13.8 W/m²), however there was no improvement in the sensible heat flux and RMSE with MED was increased
566 (from 3.9 to 4.9 W/m²). At the C₄ grass site (US-SRG), small improvements were made in the seasonal cycle of
567 both latent and sensible heat with the MED model. At the deciduous savannah site (CG-Tch) which included a
568 high proportion of shrub PFT in the land cover type used in the site simulation, large improvements in the seasonal
569 cycle of both fluxes were simulated with the MED model, as a result of a decrease in the latent heat flux and an
570 increase in the sensible heat flux (RMSE decreased from 39.5/31.6 to 30.4/24.4 W/m² for latent/sensible heat
571 respectively).



572

573 **Figure 2.** Comparison of simulated g_s with MED (y axis) versus JAC (x axis) for all five JULES PFTs at one grid
574 point (lat: 48.25; lon: 5.25) shown are hourly values for the year 2000 (see SI section S3 for further details).

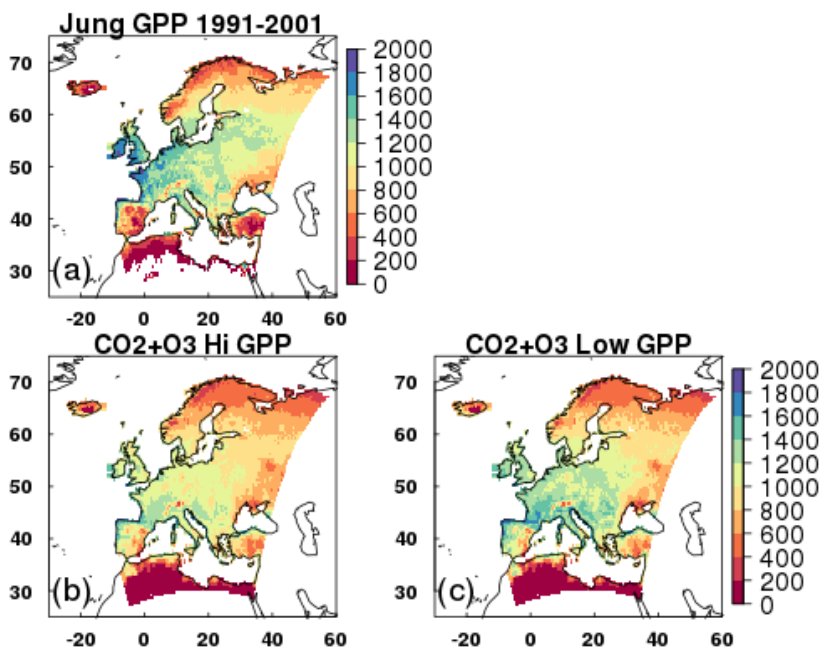
575

576 3.2 Evaluation of the JULES O₃ model

577 For all JULES scenarios similar spatial patterns of GPP are simulated compared to MTE (Fig. 3 and Fig. S13).
578 MTE estimates a mean GPP for present day in Europe of 938 gC m² yr⁻¹ (Fig. 3). JULES tends to under-predict
579 GPP relative to the MTE product, estimates of GPP from JULES with both transient CO₂ and O₃ (CO₂+O₃
580 simulation) gives a mean across Europe of 813 gC m² yr⁻¹ (high plant O₃ sensitivity) to 881 gC m² yr⁻¹ (low plant

581 O₃ sensitivity), both of which are significantly different to the MTE product ($t=27$, $d.f.=5750$, $p<2.2e^{-16}$ (high);
 582 $t=4.3$, $d.f.=5750$, $p<1.5e^{-05}$ (low); Fig. 3). Forcing with CO₂ alone (CO₂ simulation) gives a mean GPP across
 583 Europe of 900 to 923 gC m² yr⁻¹ (high and low plant O₃ sensitivity respectively), and O₃ alone (O₃ simulation -
 584 without the protective effect of CO₂) reduces estimated GPP to 732 to 799 gC m² yr⁻¹ (Fig. S13). At latitudes
 585 >45°N JULES has a tendency to under-predict MTE-GPP, and at latitudes <45°N JULES tends to over-predict
 586 MTE-GPP (Fig. S14). These regional differences are highlighted in Fig. S15, where in the Mediterranean region,
 587 JULES tends to over-predict compared to MTE-GPP, so simulations with O₃ reduce the simulated GPP bringing
 588 it closer to MTE. In the temperate region however, JULES tends to under-estimate MTE-GPP, so the addition of
 589 O₃ reduces simulated GPP further (Fig. S15). In the boreal region, JULES under-predicts GPP, but to a lesser
 590 extent than in the temperate region, and the addition of O₃ has less impact on reducing the GPP further (Fig. S15).

591



592
 593 **Figure 3.** Mean GPP (g C m² yr⁻¹) from 1991 to 2001 for a) the observationally based globally extrapolated Flux
 594 Network model tree ensemble (MTE) (Jung *et al.*, 2011); b, c) model simulations with transient CO₂ and transient
 595 O₃ (CO₂+O₃), high and low plant O₃ sensitivity respectively.

596

597

598 3.3 European simulations - Historical Period: 1901-2001

599

600 Over the historical period (1901-2001), O₃ (O₃ simulation) reduced GPP under both the low and high plant O₃
 601 sensitivity parameterizations by -3% to -9% respectively (Table 1), and this difference in simulated GPP was
 602 significant ($t=102.2$, $d.f.=6270$, $p<2.2e^{-16}$). Figure 4 highlights regional variations, however, where simulated
 603 reductions in GPP are up to 20% across large areas of Europe, and up to 30% in some Mediterranean regions
 604 under the high plant O₃ sensitivity. Some Boreal and Mediterranean regions show small increases in GPP over

605 this period, associated with O₃ induced stomatal closure enhancing water availability in these drier regions (Fig.
606 5). This allows for greater stomatal conductance later in the year when soil moisture may otherwise have been
607 limiting to growth (up to 10%, Fig. 5), and therefore higher GPP, but these regions comprise only a small area of
608 the entire domain. Indeed, over much of the Europe, O₃-induced stomatal closure led to reduced g_s (up to 20%)
609 across large areas of temperate Europe and the Mediterranean, and even greater reductions in some smaller regions
610 of southern Mediterranean (Fig. 6), and these are not associated with notable increases in soil moisture availability
611 (Fig. 5), resulting in depressed GPP over much of Europe as described above. Under the low plant O₃ sensitivity,
612 similar spatial patterns occur, but the magnitude of GPP change (up to -10% across much of Europe) and g_s change
613 (-5% to -10%) are lower compared to the high sensitivity. Over the twentieth century the land carbon sink is
614 suppressed (-2% to -6%, Table 1). Large regional variation is shown in Figure 4, with temperate and
615 Mediterranean Europe seeing a large reduction in land carbon storage, particularly under the high plant O₃
616 sensitivity (up to -15%).

617

618 Combined, the physiological response to changing CO₂ and O₃ concentrations (CO₂+O₃ simulation) results in a
619 net loss of land carbon over the twentieth century under the high plant O₃ sensitivity (-2%, Table 1), dominated
620 by loss of soil carbon (Table S3). This reflects the large increases in tropospheric O₃ concentration observed over
621 this period (Fig. 1). Under the low plant O₃ sensitivity, the land carbon sink has started to recover by 2001 (+1.5%)
622 owing to the recovery of the soil carbon pool beyond 1901 values over this period (Table S3).

623

624 To gain perspective on the magnitude of the O₃ induced flux of carbon from the land to the atmosphere we relate
625 changes in total land carbon to carbon emissions from fossil fuel combustion and cement production for the EU-
626 28-plus countries from the data of Boden et al. (2013). We recognise that our simulation domain is slightly larger
627 than the EU28-plus as it includes a small area of western Russia so direct comparisons cannot be made, but this
628 still provides a useful measure of the size of the carbon flux. For the period 1970 to 1979 the simulated loss of
629 carbon from the European terrestrial biosphere due to O₃ effects on vegetation physiology was on average 1.32
630 Pg C (high vegetation sensitivity) and 0.71 Pg C (low vegetation sensitivity) (Table 2). This O₃ induced reduced
631 C uptake of the land surface is equivalent to around 8% to 16% of the emissions of carbon from fossil fuel
632 combustion and cement production over the same period for the EU28-plus countries (Table 2). Currently the
633 emissions data availability goes up to 2011, over the last observable decade (2002 to 2011) the simulated reduction
634 in land carbon due to O₃ has declined, but is still equivalent to 2% to 4% of the emissions of carbon from fossil
635 fuels and cement production for the EU28-plus countries (Table 2). By comparison with one of the largest
636 anthropogenic emissions of carbon for Europe, we show here the potential effect of O₃ on reducing the size of the
637 European land carbon sink is notable.

638

639 **3.4 European simulations - Future Period: 2001-2050**

640

641 Over the 2001 to 2050 period, region-wide GPP with O₃ only changing (O₃ simulation) increased marginally
642 (+0.1% to +0.2%, high and low plant O₃ sensitivity, Table 1, with a significant difference between the two plant
643 O₃ sensitivities ($t=57$, $d.f.=6270$ $p<2.2e^{-16}$)), although with large spatial variability as discussed below (Fig. 4g &
644 h). Figures S6 and S7 show that despite decreased tropospheric O₃ concentrations by 2050 in summer compared

645 to 2001 levels, all regions are exposed to an increase in O₃ over the wintertime, and some regions of Europe,
646 particularly temperate/Mediterranean experience increases in O₃ concentration in spring and autumn. Therefore,
647 although in the O₃ simulation, overall simulated GPP for Europe shows a small increase, large spatial variability
648 is shown in Fig's 4g & h because of the variability in O₃ concentration with region and season. Increased GPP
649 (dominantly 10%, but up to 20% in some areas) on 2001 levels is simulated across areas of Europe, however,
650 decreases of up to 21% are simulated in some areas of the Mediterranean, up to 15% in some areas of the boreal
651 region and up to 27% in the temperate zone (Fig. 4g & h).

652

653 When O₃ and CO₂ effects are combined (CO₂+O₃ simulation), simulated GPP increases (+15% to +18%,
654 high/low plant O₃ sensitivities respectively, Table 1). This increase is greater than the enhancement simulated
655 when CO₂ affects plant growth independently (CO₂ simulation), because additional O₃ induced stomatal closure
656 increases soil water availability in some regions, which enhances growth more in the CO₂+O₃ simulation,
657 compared to the CO₂ simulation. Nevertheless, although the percentage gain is larger, the absolute value of GPP
658 by 2050 remains lower in CO₂+O₃ compared to GPP in the CO₂ simulations, highlighting the negative impact of
659 O₃ at the land surface (Table S4).

660

661 Despite small increases in GPP in the O₃ simulation, the land carbon sink continues to decline from 2001 levels
662 (-0.7% to -1.6%, low and high plant O₃ sensitivity respectively, Table 1). This is because the soil and vegetation
663 carbon pools continue to lose carbon as they adjust slowly to small changes in input (GPP), i.e. the soil carbon
664 pool is not in equilibrium in 2001, and is declining in response to reduced litter input as a result of 20th C O₃
665 impacts on GPP. Nevertheless, the negative effect of O₃ on the future land sink is markedly reduced relative to
666 the historical period. Figure 4e & f however highlights regional differences. Boreal regions and parts of central
667 Europe see minimal O₃ damage, whereas some areas of southern and northern Europe see further losses of up to
668 8% on 2001 levels. The CO₂+O₃ simulation are dominated by the physiological effects of changing CO₂, with
669 land carbon sink increases of up to 7% (Table 1).

670

671 **3.5 European simulations – Full experimental period: 1901-2050**

672

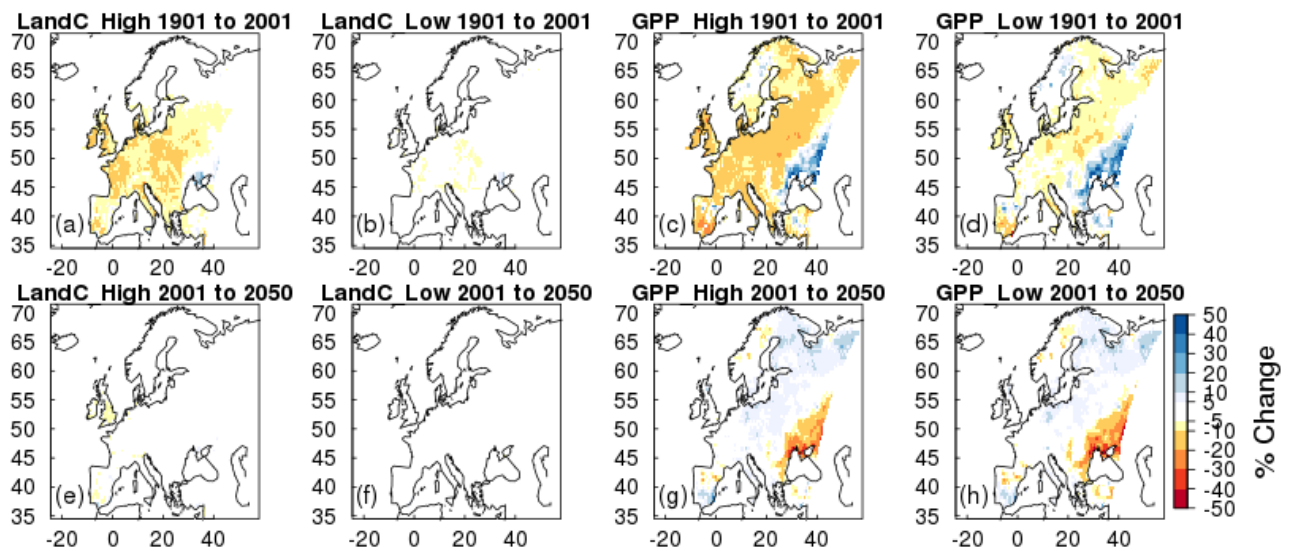
673 From 1901 to 2050, the O₃ simulation reduces GPP (-4% to -9%, with a significant difference between the low
674 and high plant O₃ sensitivity ($t=95, d.f.=6270, p<2.2e^{-16}$)) and land carbon storage (-3% to -7%, Table 1).
675 Regionally, O₃ damage is lowest in the boreal zone, GPP decreases are largely between 5% to 8% / 2% to 4% for
676 the high/low plant O₃ sensitivity respectively, with large areas minimally affected by O₃ damage (Figure 7),
677 consistent with lower g. of needle leaf trees that dominate this region, and so lower O₃ uptake (Fig. S16 & S17).
678 In the temperate region, O₃ damage is extensive with reductions in GPP dominantly from 10% to 15% for the low
679 and high plant O₃ sensitivity respectively. Across significant areas of this region reductions in GPP are up to 20%
680 under high plant O₃ sensitivity (Figure 7). In the Mediterranean region, O₃ damage reduces GPP by 5% to 15% /
681 3% to 6% for the high/low plant O₃ sensitivity respectively, with some areas seeing greater losses of up to 20%
682 under the high plant O₃ sensitivity, but this is less extensive than that seen in the temperate zone (Figure 7). In
683 these drier regions, O₃ induced stomatal closure can increase available soil moisture (Fig. S16 & S17).

684

685 The CO₂+O₃ simulation shows that CO₂ induced stomatal closure can help alleviate O₃ damage by reducing the
 686 uptake of O₃ (Table S6). In these simulations, CO₂-induced stomatal closure was found to offset O₃-suppression
 687 of GPP, such that GPP by 2050 is 3% to 7% lower due to O₃ exposure (CO₂+O₃), rather than 4% to 9% lower in
 688 the absence of increasing CO₂ (O₃ simulation, Table S6). Figure 6 shows this spatially, O₃ damage is reduced
 689 when the effect of atmospheric CO₂ on stomatal closure is accounted for, however despite this, the land carbon
 690 sink and GPP remain significantly reduced due to O₃ exposure.

691
 692 From 1901 to 2050, the CO₂+O₃ simulation results in an increase in European land carbon uptake (+5% to +9%),
 693 and an increase in GPP (+20% to +23%) by 2050 for the high and low plant O₃ sensitivity, respectively (Table 1).
 694 Nevertheless, despite this increase there remains a large negative impact of O₃ on the European land carbon sink
 695 (Fig. S18). By 2050 the simulated enhancement of land carbon and GPP in response to elevated CO₂ alone (CO₂
 696 simulation) is reduced by 3% to 6% (land carbon) and 4% to 9% (GPP) for the low and high plant O₃ sensitivity
 697 respectively, when O₃ is also accounted for (CO₂+O₃ simulation, Table 1). This is a large reduction in the ability
 698 of the European terrestrial biosphere to sequester carbon.

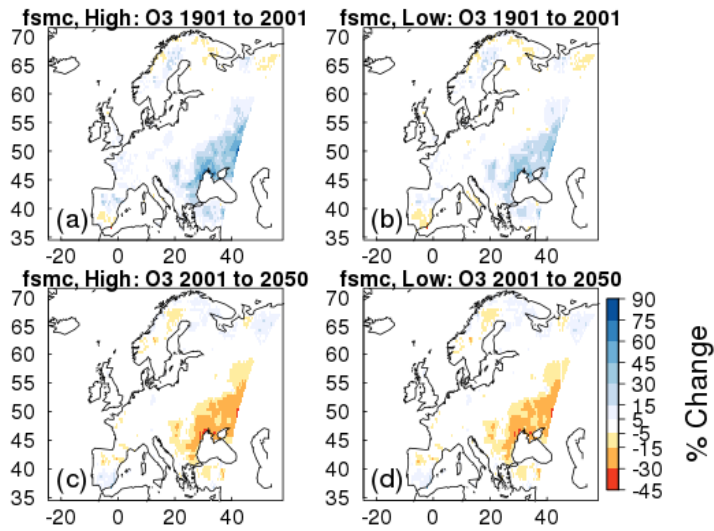
699



700

701 **Figure 4.** Simulated percentage change in total carbon stocks (Land C) and gross primary productivity (GPP) due
 702 to O₃ effects at fixed pre-industrial atmospheric CO₂ concentration (O₃ simulation). Changes are shown for the
 703 periods 1901 to 2001, and 2001 to 2050 for the high and low plant O₃ sensitivity.

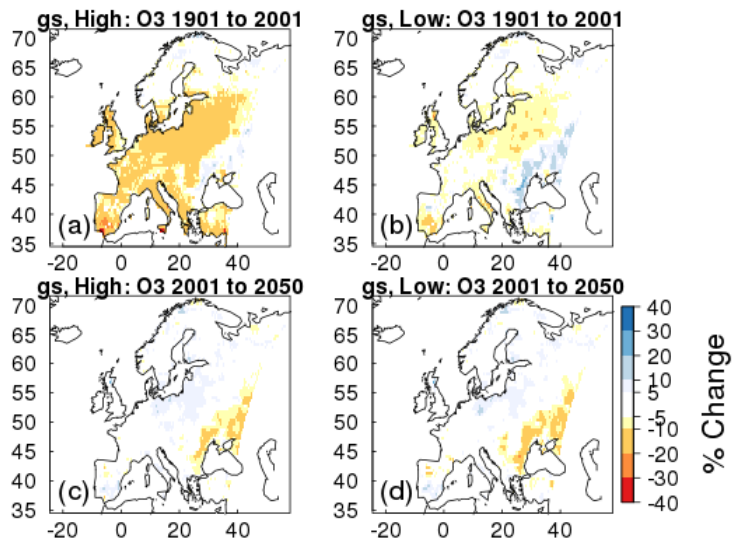
704



705

706 **Figure 5.** Simulated percentage change in plant available soil moisture (*fsmc*) due to O_3 effects at fixed pre-
 707 industrial atmospheric CO_2 concentration (O_3 simulation). Changes are shown for the periods 1901 to 2001, and
 708 2001 to 2050 for the high and low plant O_3 sensitivity.

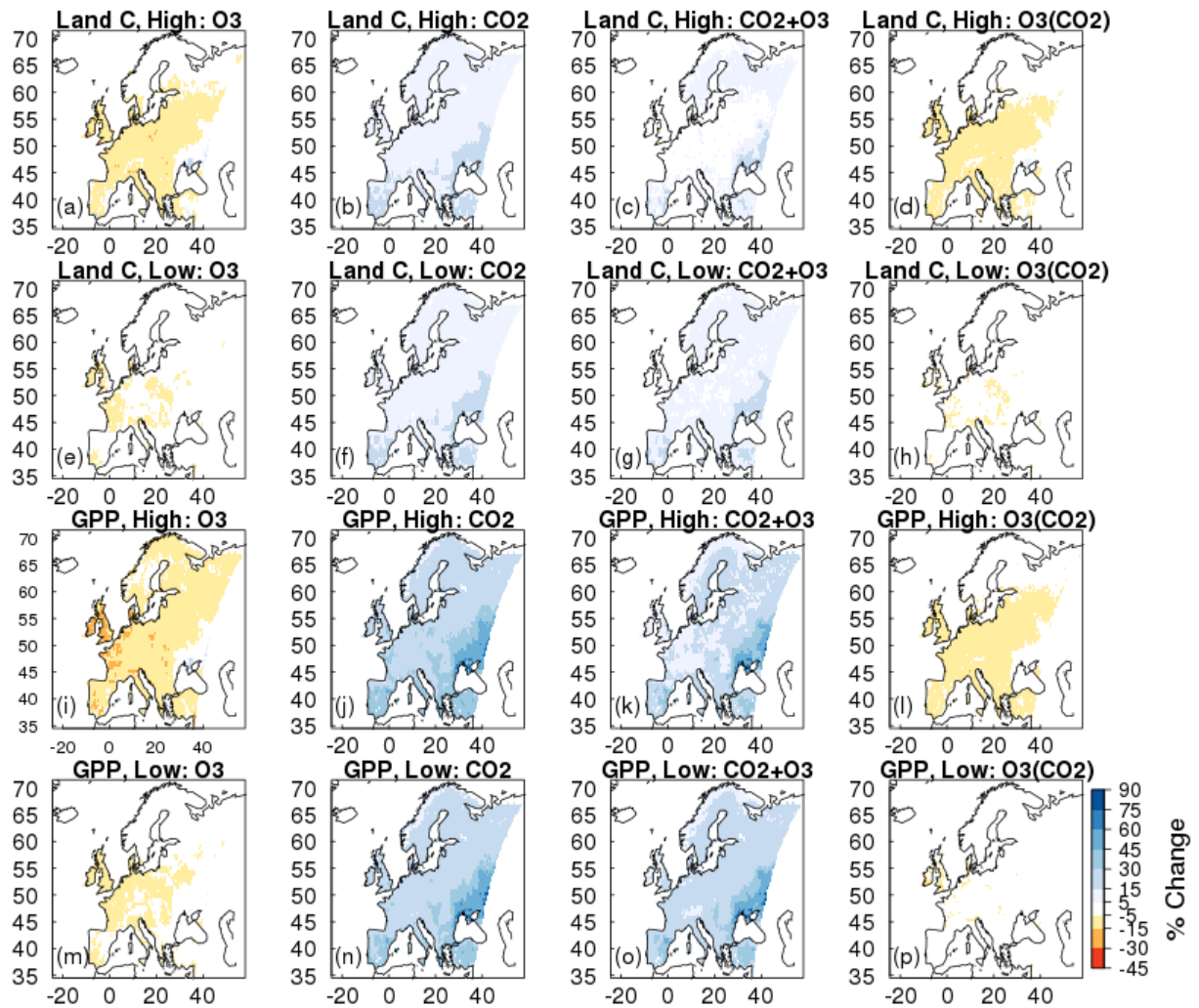
709



710

711 **Figure 6.** Simulated percentage change in stomatal conductance (*gs*) due to O_3 effects at fixed pre-
 712 industrial atmospheric CO_2 concentration (O_3 simulation). Changes are shown for the periods 1901 to 2001, and
 713 2001 to 2050 for the high and low plant O_3 sensitivity.

714



715

716 **Figure 7.** Simulated percentage change in total carbon stocks (Land C) and gross primary productivity (GPP) due
 717 to i) (a, e, i, m) O₃ effects at fixed pre-industrial atmospheric CO₂ concentration (O₃ simulation), ii) (b, f, j, n)
 718 CO₂ fertilisation at fixed pre-industrial O₃ concentration (CO₂ simulation), iii) (c, g, k, o) the interaction between
 719 O₃ and CO₂ effects (CO₂+O₃ simulation) iv) (d, h, l, p) O₃ effects with changing atmospheric CO₂ concentration
 720 (i.e. O₃ damage accounting for the effect of CO₂ induced stomatal closure; CO₂+O₃ – CO₂). Changes are depicted
 721 for the periods 1901 to 2050 for high and lower ozone plant sensitivity.

722

723

724

725

726

727

728

	High Plant O₃ Sensitivity					
	1901 - 2001		2001 - 2050		1901 - 2050	
	GPP (Pg C yr ⁻¹)	Land C (Pg C)	GPP (Pg C yr ⁻¹)	Land C (Pg C)	GPP (Pg C yr ⁻¹)	Land C (Pg C)
Value in 1901:	9.05	167	-	-	9.05	167
Absolute Change:						
O₃	-0.81	-9.21	0.01	-2.44	-0.80	-11.65
CO₂	1.16	4.24	1.42	12.98	2.58	17.22
CO₂ + O₃	0.13	-3.28	1.66	11.11	1.79	7.83
% Change:						
O₃	-8.95	-5.51	0.12	-1.55	-8.84	-6.98
CO₂	12.82	2.54	13.91	7.58	28.51	10.31
CO₂ + O₃	1.44	-1.96	18.08	6.79	19.78	4.69
	Low Plant O₃ Sensitivity					
	1901 - 2001		2001 - 2050		1901 - 2050	
	GPP (Pg C yr ⁻¹)	Land C (Pg C)	GPP (Pg C yr ⁻¹)	Land C (Pg C)	GPP (Pg C yr ⁻¹)	Land C (Pg C)
Value in 1901:	9.34	167.5	-	-	9.34	167.5
Absolute Change:						
O₃	-0.30	-3.59	0.02	-1.07	-0.40	-4.66
CO₂	1.15	6.43	1.35	13.14	2.50	19.57
CO₂ + O₃	0.65	2.50	1.50	12.35	2.15	14.85
% Change:						
O₂	-3.21	-2.14	0.22	-0.65	-4.28	-2.78
CO₂	12.31	3.84	12.87	7.55	26.77	11.68
CO₂ + O₃	6.96	1.49	15.02	7.26	23.02	8.87

729

730 **Table 1.** Simulated changes in the European land carbon cycle due to changing O₃ and CO₂ concentrations
731 (independently and together). Shown are changes in total carbon stocks (Land C) and gross primary productivity
732 (GPP), over three different periods (historical: 1901 to 2001, future: 2001 to 2050, and full time series: 1901 to
733 2050). Absolute (top) and relative (bottom) differences are shown. For 2001 to 2050, please refer to Table S4 for
734 the initial value for each run. See the SI for details of the estimation of the O₃ and CO₂ effects and their interaction.

735

736

737

738

739

740

741

742

743

744

	Mean (Pg C)				
	1970-1979	1980-1989	1990-1999	2000-2009	2002-2011
Modelled O₃ effect on land C sink :					
Higher sensitivity	-1.32	-1.01	-0.97	-0.53	-0.50
Low sensitivity	-0.71	-0.58	-0.50	-0.29	-0.26
Sum of C emissions from fossil fuel combustion and cement production (Pg C)					
	8.39	8.63	12.26	12.83	12.75
C lost from O₃ effect as a % of fossil fuel and cement emissions (%):					
Higher sensitivity	-15.73	-11.70	-7.91	-4.13	-3.92
Low sensitivity	-8.46	-6.72	-4.08	-2.26	-2.04

745

746 **Table 2.** Simulated change in total land carbon due to O₃ damage with changing atmospheric CO₂ concentration
747 for the two vegetation sensitivities. The sum of carbon emissions for each decade from fossil fuel combustion and
748 cement production for the EU-28 countries plus Albania, Bosnia and Herzegovina, Iceland, Belarus, Serbia,
749 Moldova, Norway, Turkey, Ukraine, Switzerland and Macedonia (EU28-plus) are shown, the data is from Boden
750 *et al.*, 2013. The simulated change in land carbon as a result of O₃ damage is depicted as a percentage of the EU28-
751 plus emissions to demonstrate the magnitude of the additional source of carbon to the atmosphere from plant O₃
752 damage.

753

754 4 Discussion

755

756 4.1 Evaluation of g_s models and JULES O₃ model

757

758 Comparison of the new g_s model implemented in this study (MED) with the g_s model currently used as standard
759 in JULES (JAC) revealed large differences in g_s for each PFT, principally as a result of the data-based
760 parameterisation of the new model. Water use increased for the broadleaf tree and C₃ herbaceous PFTs using the
761 MED model compared to JAC, but decreased for the needle leaf tree, C₄ herbaceous and shrub PFTs which
762 displayed a more conservative water use strategy compared to JAC. These changes are in line with the work of
763 De Kauwe *et al.* (2015) who found a reduction in annual transpiration for evergreen needle leaf, tundra and C₄
764 grass regions when implementing the Medlyn g_s model into the Australian land surface scheme CABLE. Site-
765 level evaluation of the models against Fluxnet observations showed that in general the MED model improved
766 simulated seasonal cycles of latent and sensible heat. The magnitude of the improvement varied with site, large
767 improvements were seen at the deciduous savanna site, and at the NT sites and BT site (US_UMB) in the spring
768 and summer. However, much smaller improvements were seen at the grass sites. Changes in g_s in this study
769 resulted in differences in latent and sensible heat fluxes. Changes in the partitioning of energy fluxes at the land
770 surface could have consequences for the intensity of heatwaves (Cruz *et al.*, 2010; Kala *et al.*, 2016), runoff (Betts
771 *et al.*, 2007; Gedney *et al.*, 2006) and rainfall patterns (de Arellano *et al.*, 2012), although fully coupled simulations
772 would be necessary to detect these effects. The differences in simulated g_s led to differences in uptake of O₃
773 between the two models because the rate of g_s is the predominant determinant of the flux of O₃ through stomata.

774 Higher O₃ uptake is indicative of greater damage. Therefore, given that C₃ herbaceous vegetation is the dominant
775 land cover class across the European domain used in this study, this suggests a greater O₃ impact for Europe would
776 be simulated with MED model compared to JAC in our simulations where chemistry is uncoupled from the land
777 surface.

778

779 We evaluated the JULES O₃ model by comparing modelled GPP against the Jung et al (2011) MTE product.
780 Similar spatial patterns of GPP were simulated by JULES compared to MTE. Zonal means also showed similar
781 patterns of GPP, although JULES under predicted GPP compared to MTE at latitudes >45°N (temperate and boreal
782 regions; all simulations) and over predicted GPP at latitudes <45°N (Mediterranean region; all simulations). The
783 simulations with transient O₃ (i.e. O₃ and CO₂+O₃) showed large differences in GPP between the high and low
784 plant O₃ sensitivity simulations, this is to be expected given that the high plant O₃ sensitivity simulations were
785 parameterised to be ‘damaged’ more by O₃, i.e. greater reduction of photosynthesis/g_s with O₃ exposure compared
786 to the low plant O₃ sensitivity simulations. This difference was largest in the temperate zone, largely because of
787 C₃ grass cover being the dominant land cover here and the difference in the sensitivity to O₃ between the high and
788 low calibrations is significantly larger for C₃ grasses compared to the needle leaf trees that dominate in the boreal
789 region. Additionally, a longer growing season in the temperate region may allow for greater uptake of O₃ into
790 vegetation. C₃ grass is also the dominant land cover in the Mediterranean region with a different calibration used
791 for Mediterranean grasses for the low plant O₃ sensitivity which is less sensitive to O₃ than the temperate C₃
792 grasses, but high soil moisture stress is common throughout the growing season in the Mediterranean limiting the
793 uptake of O₃ through stomata, which likely diminishes the difference between the high and low calibrations.

794

795 **4.2 Lower than expected O₃ damage?**

796

797 Our estimates suggest present day O₃ reduced GPP by 3% to 9% on average across Europe and NPP by 5% to
798 11% (Table S3). Anav et al. (2011) simulated a 22% reduction of GPP across Europe for 2002 using the
799 ORCHIDEE model. Present day O₃ exposure reduced GPP by 10% to 25% in Europe, and 10.8% globally in the
800 study by Lombardozzi et al. (2015) using the Community land model (CLM). O₃ reduced NPP by 11.2% in Europe
801 from 1989 to 1995 using the Terrestrial Ecosystem Model (TEM) (Felzer et al., 2005). Globally, concentrations
802 of O₃ predicted for 2100 reduced GPP by 14% to 23% using a former parameterisation of O₃ sensitivity in JULES
803 (Sitch et al., 2007). The recent study by Franz et al. (2017) showed mean GPP declined by 4.7% over the period
804 2001 to 2010 using the OCN model over the same European domain and using the same O₃ forcing produced by
805 EMEP MSC-W as used in this study. Our estimates of changes in current day GPP and NPP are at the lower end
806 of previously modelled estimates. Simulated O₃ impacts will depend in a large part on the scenario of O₃
807 concentrations used as forcing, meteorological forcing and how sensitive vegetation is parameterised to be to O₃
808 damage, in addition to the different process representation of O₃ damage in each model. It is therefore difficult to
809 hypothesise as to exactly why modelled estimates differ, but suggests that an ensemble approach to modelling O₃
810 impacts on the terrestrial biosphere would be beneficial to understand some of these differences and provide
811 estimates of O₃ damage with uncertainties.

812

813 4.3 Impacts of O₃ at the land surface

814

815 In this study, O₃ has a detrimental effect on the size of the land carbon sink for Europe. This is primarily through
816 a decrease in the size of the soil carbon pool as a result of reduced litter input to the soil, consistent with reduced
817 GPP/NPP. Field studies show that in some regions of Europe, soil carbon stocks are decreasing (Bellamy et al.,
818 2005;Capriel, 2013;Heikkinen et al., 2013;Sleutel et al., 2003). The study of Bellamy et al. (2005), for example,
819 showed that carbon was lost from soils across England and Wales between 1978 to 2003 at a mean rate of 0.6%
820 per year with little effect of land use on the rate of carbon loss, suggesting a possible link to climate change. It is
821 understood that climate change is likely to affect soil carbon turnover. Increased temperatures increase microbial
822 decomposition activity in the soil, and therefore increase carbon losses through higher rates of respiration (Cox et
823 al., 2000;Friedlingstein et al., 2006;Jones et al., 2003). However, some studies have found that O₃ can decrease
824 soil carbon content. Talhelm et al. (2014), for example, found O₃ reduced carbon content in near surface mineral
825 soil of forest soils exposed to 11 years of O₃ fumigation. Hofmockel et al. (2011) found elevated O₃ reduced the
826 carbon content in more stable soil organic matter pools, and Loya et al. (2003) showed that the fraction of soil
827 carbon formed in forest soils over a 4 year experimental period when fumigated with both CO₂ and O₃ was reduced
828 by 51% compared to the soil fumigated with CO₂ alone. It is agreed that amongst other factors that change with
829 O₃ exposure such as litter quality and composition, reduced litter quantity also has significant detrimental
830 consequences for soil carbon stocks (Andersen, 2003;Lindroth, 2010;Loya et al., 2003). Results from this study
831 therefore suggest that increasing tropospheric O₃ may be a contributing factor to the declining soil carbon stocks
832 observed across Europe as a result of reduced litter input to the soil carbon pool consistent with reduced NPP.

833

834 We acknowledge, however, that our model simulations do not include coupling of Nitrogen and Carbon cycles,
835 or land management practices. We include a representation of agricultural regions through the model calibration
836 against the wheat O₃ sensitivity function (CLRTAP, 2017), and in our simulations the high plant O₃ sensitivity
837 scenario uses this calibration against wheat for all C₃/C₄ land cover which dominates our model domain. Wheat is
838 known to be one of the most O₃ sensitive crop species however, so it is possible that our simulations over-estimate
839 the O₃ impact at the land surface. However, the low plant O₃ sensitivity calibration against natural grasslands
840 provides a counter estimate of the impact of O₃ at the land surface, therefore it is important to consider the range
841 our results provide (i.e. both the high and low plant O₃ sensitivity) as an indicator of the impact of O₃ on the land
842 surface. As with all uncoupled modelling studies, a change in g_s and flux will impact the O₃ concentration itself.
843 Therefore adopting the Medlyn formulation with a higher g_s and subsequently higher O₃ flux for broadleaf and C₃
844 PFTs (Fig 2) would lead to reduced O₃ concentration, which in turn would act to dampen the effect of higher g_s
845 on O₃ flux, although the higher uptake of O₃ by vegetation may lead to more damage and increase O₃
846 concentrations, in an uncoupled chemistry-land modelling system such as this it is not possible to predict which
847 process would dominate. Additionally, this version of JULES does not have a crop module; it has no land
848 management practices such as harvesting, ploughing or crop rotation – processes which may have counteracting
849 effects on the land carbon sink. Further, without a coupled Carbon and Nitrogen cycle, it is likely that the CO₂
850 fertilisation response of GPP and the land carbon sink is over estimated in some regions of our simulations since
851 nitrogen availability limits terrestrial carbon sequestration of natural ecosystems in the temperate and boreal zone

852 (Zaehle, 2013). This would have consequences for our modelled O₃ impact, particularly into the future where the
853 large CO₂ fertilisation effect was responsible for partly offsetting the negative impact of O₃. Although in our
854 simulations a high fraction of land cover is agricultural which we assume would be optimally fertilised. Our
855 simulations also use a fixed climate, so we do not include the effect of climate change on shifting plant phenology.
856 Therefore, our results may underestimate plant O₃ damage, since if the growing season started earlier or finished
857 later, plants in some regions would be exposed to higher O₃ concentrations. Nevertheless, we emphasise that this
858 study provides a sensitivity assessment of the impact of plant O₃ damage on GPP and the land carbon sink.

859
860 Another caveat we fully acknowledge is that at the leaf-level JULES is parameterised to reduce g_s with O₃
861 exposure. Whilst this response is commonly observed (Wittig et al., 2007; Ainsworth et al., 2012), there is evidence
862 to suggest that O₃ impairs stomata in some species, making them non-responsive to environmental stimuli (Hayes
863 et al., 2012; Hoshika et al., 2012a; Mills et al., 2009; Paoletti and Grulke, 2010). In drought conditions the
864 mechanism is thought to involve O₃ stimulated ethylene production which interferes with the stomatal response
865 to ABA signalling (Wilkinson and Davies, 2009; Wilkinson and Davies, 2010). Such stomatal sluggishness can
866 result in higher O₃ uptake and injury, increased water-loss, and therefore greater vulnerability to environmental
867 stresses (Mills et al., 2016). McLaughlin (2007a; 2007b) and Sun et al. (2012) provide evidence of increased
868 transpiration and reduced streamflow in forests at the regional scale in response to ambient levels of O₃, and
869 suggest this could increase the frequency and severity of droughts. Hoshika et al. (2012b) however found that
870 despite sluggish stomatal control in O₃ exposed trees, whole tree water use was lower in these trees because of
871 lower gas exchange and premature leaf shedding of injured leaves. To our knowledge, the study of Hoshika et al.
872 (2015) is the first to include an explicit representation of sluggish stomatal control in a land-atmosphere model,
873 they show that sluggish stomatal behaviour has implications for carbon and water cycling in ecosystems.
874 However, it is by no means a ubiquitous response, and it is not fully understood which species respond this way
875 and under what conditions (Mills et al., 2016; Wittig et al., 2007). Nevertheless, this remains an important area of
876 future work.

877
878 In this work we implement the stomatal closure proposed in Medlyn et al., (2011), this uses the parameter g_l .
879 Hoshika et al. (2013) show a significant difference in the g_l parameter (higher in elevated O₃ compared to ambient)
880 in Siebold's beech in June of their experiment. However, this is only at the start of the growing season, further
881 measurements show no difference in this parameter between O₃ treatments. Quantifying an O₃ effect directly on
882 g_l would require a detailed meta-analysis of empirical data on photosynthesis and g_s for different PFTs, which is
883 currently lacking in the literature. With such information lacking, here we take an empirical approach to modelling
884 plant O₃ damage, essentially by applying a reduction factor to the simulated plant photosynthesis based on
885 observations of whole plant losses of biomass with accumulated O₃ exposure, for which there is a lot more
886 available data (e.g. CLRTAP, 2017).

887
888 The calculation of O₃ deposition in the EMEP model uses the stomatal conductance formulation presented in
889 Emberson et al. (2000; 2001), which depends on temperature, light, humidity and soil moisture (commonly
890 referred to as DO₃SE). Because we link two different model systems, the g_s values in the EMEP model differ from
891 those obtained using the Medlyn formulation. We acknowledge this inconsistency as a caveat of our study,

892 however comparison of g_{max} (maximum g_s) values from both models (EMEP (g_{max} is an input parameter
893 determining the maximum g_s) and JULES (g_{max} is not used as an input parameter in JULES, instead we calculated
894 g_{max} for each PFT taking the mean across the model domain for the year 2001) suggests the differences are small
895 for deciduous forest (EMEP 150-200, JULES ~180, all units in $\text{mmol O}_3/\text{m}^2$ (PLA)/s), and C_3/C_4 crops (EMEP
896 270-300, JULES ~260-390), but are larger for coniferous forest (EMEP 140-200, JULES ~60-70) and shrubs
897 (EMEP 60-200, JULES 360-390). It should be noted that the role of EMEP in this study is not to provide g_s , but
898 to provide O_3 at the top of the vegetation canopy. This firstly entails a calculation of the large-scale ozone
899 concentrations for Europe, which are represented by the gridded values of grid-cell average concentration, and
900 secondly to calculate the vertical gradients between these grid-cell centres (at ca. 45m) and the top of the
901 vegetation canopy. O_3 deposition is important for both steps; it is known to have a substantial impact on the
902 lifetime and concentrations of O_3 in the planetary boundary layer (Garland and Derwent, 1979; Val Martin et al.,
903 2014), and also in determining the local vertical gradients above different land-covers (CLRTAP, 2017; Gerosa et
904 al., 2017; Tuovinen et al., 2009). Vertical gradients between the 45m level and the top of forest canopies tend to
905 be limited (Fuentes et al., 2007; Karlsson et al., 2006) due to the good mixing normally induced by forest
906 roughness. Vertical gradients between 45m and the top of shorter vegetation such as grasslands or crops can be
907 larger however (CLRTAP, 2017; Gerosa et al., 2017). Accounting for such land-cover specific gradient effects has
908 been shown to have large impacts on estimates of O_3 metrics (Simpson et al., 2007).

909

910

911 These offline simulations show the sensitivity of GPP and the land carbon sink to tropospheric O_3 , suggesting that
912 O_3 is an important predictor of future GPP and the land carbon store across Europe. There are uncertainties in our
913 estimates however from the use of uncoupled tropospheric chemistry, meteorology and stomatal function. For
914 example, increased frequency of drought in the future would reduce stomatal conductance (assuming no sluggish
915 stomatal response) and thus O_3 uptake. Since our offline simulations do not include this feedback it is possible the
916 O_3 effect is over estimated here. Given the complexity of potential interactions and feedbacks it remains difficult
917 to diagnose the importance of individual factors (e.g. the direct physiological response) in a fully coupled
918 simulation. Once the importance of a process is demonstrated offline, it provides evidence of the need to
919 incorporate such process in coupled regional and global simulations.

920

921 **4.4 O_3 as a missing component of carbon cycle assessments?**

922

923 Comprehensive analyses of the European carbon balance suggest a large biogenic carbon sink (Janssens et al.,
924 2003; Luyssaert et al., 2012; Schulze et al., 2009). However, estimates are hampered by large uncertainties in key
925 components of the land carbon balance, such as estimates of soil carbon gains and losses (Ciais et al.,
926 2010; Janssens et al., 2003; Schulze et al., 2009; Schulze et al., 2010). We suggest that the effect of O_3 on plant
927 physiology is a contributing factor to the decline in soil carbon stores observed across Europe, and as such this O_3
928 effect is a missing component of European carbon cycle assessments. Over the full experimental period (1901 to
929 2050), our results show elevated O_3 concentrations reduce the amount of carbon that can be stored in the soil by
930 3% to 9% (low and high plant O_3 sensitivity, respectively), which almost completely offsets the beneficial effects
931 of CO_2 fertilisation on soil carbon storage under the high plant O_3 sensitivity. This would contribute to a change

932 in the size of a key carbon sink for Europe, and is particularly important when we consider the evolution of the
933 land carbon sink into the future given the impact of O₃ on soil carbon sequestration and the high uncertainty of
934 future tropospheric O₃ concentrations. Schulze et al. (2009) and Luysaert et al. (2012) extended their analysis of
935 the European carbon balance to include additional non-CO₂ greenhouse gases (CH₄ and N₂O). Both studies found
936 that emissions of these offset the biogenic carbon sink, reducing the climate mitigation potential of European
937 ecosystems. This highlights the importance of accounting for all fluxes and stores in carbon/greenhouse gas
938 balance assessments, of which O₃ and its indirect effect on the CO₂ flux via direct effects on plant physiology is
939 currently missing.

940

941 **4.5 The interaction between O₃ and CO₂**

942

943 We looked at the interaction between CO₂ and O₃ effects. Our results support the hypothesis that elevated
944 atmospheric CO₂ provides some protection against O₃ damage because of lower g_s that reduces uptake of O₃
945 through stomata (Harmens et al., 2007; Wittig et al., 2007). In the present study, reductions in GPP and the land
946 carbon store due to O₃ exposure were lower when simulated with concurrent changes in atmospheric CO₂. Despite
947 acclimation of photosynthesis after long-term exposure to elevated atmospheric CO₂ of field grown plants
948 (Ainsworth and Long, 2005; Medlyn et al., 1999), there is no evidence to suggest that g_s acclimates (Ainsworth et
949 al., 2003; Medlyn et al., 2001). This suggests the protective effect of elevated atmospheric CO₂ against O₃ damage
950 will be sustained in the long term. However, although meta-analysis suggest a general trend of reduced g_s with
951 elevated CO₂ (Ainsworth and Long, 2005; Medlyn et al., 1999), this is not a universal response. Stomatal responses
952 on exposure to elevated CO₂ with FACE treatment varied with genotype and growth stage in a fast-growing poplar
953 community (Bernacchi et al., 2003; Tricker et al., 2009). In other mature forest stands, limited stomatal response
954 to elevated CO₂ was observed after canopy closure (Ellsworth, 1999; Uddling et al., 2009). Also, some studies
955 found that stomatal responses to CO₂ were significant only under high atmospheric humidity (Cech et al.,
956 2003; Leuzinger and Körner, 2007; Wullschleger et al., 2002). These examples illustrate that stomatal responses to
957 elevated atmospheric CO₂ are not universal, and as such the protective effect of CO₂ against O₃ injury cannot be
958 assumed for all species, at all growth stages under wide ranging environmental conditions.

959

960 **5 Conclusion**

961

962 What is abundantly clear is that plant responses to both CO₂ and O₃ are complicated by a host of factors that are
963 only partly understood, and it remains difficult to identify general, global patterns given that effects of both gases
964 on plant communities and ecological interactions are highly context and species specific (Ainsworth and Long,
965 2005; Fuhrer et al., 2016; Matyssek et al., 2010b). This study quantifies the sensitivity of the land carbon sink for
966 Europe and GPP to changing concentrations of atmospheric CO₂ and O₃ from 1901 to 2050. We have used a state
967 of the art land surface model calibrated for European vegetation to give our best estimates of this sensitivity within
968 the limits of data availability to calibrate the model for O₃ sensitivity, current knowledge and model structure. In
969 summary, this study has shown that potential gains in terrestrial carbon sequestration over Europe resulting from
970 elevated CO₂ can be partially offset by concurrent rises in tropospheric O₃ over 1901-2050. Specifically, we have
971 shown that the negative effect of O₃ on the land carbon sink was greatest over the twentieth century, when O₃

972 concentrations increased rapidly from pre-industrial levels. Over this period soil carbon stocks were diminished
973 over agricultural areas, consistent with reduced NPP and litter input. This loss of soil carbon was largely
974 responsible for the decrease in the size of the land carbon sink over Europe. The O₃ effect on the land carbon store
975 and flux was reduced into the future as CO₂ concentration rose considerably and changes in O₃ concentration were
976 less pronounced. However, there remained a large cumulative negative impact on the land carbon sink for Europe
977 by 2050. The interaction between the two gases was found to reduce O₃ injury owing to reduced stomatal opening
978 in elevated atmospheric CO₂. However, primary productivity and land carbon storage remained suppressed by
979 2050 due to plant O₃ damage. Expressed as a percentage of the emissions from fossil fuel and cement production
980 for the EU28-plus countries, the carbon emissions from O₃-induced plant injury are a source of anthropogenic
981 carbon previously not accounted for in carbon cycle assessments. Our results demonstrate the sensitivity of
982 modelled terrestrial carbon dynamics to the direct effect of tropospheric O₃ and its interaction with atmospheric
983 CO₂ on plant physiology, demonstrating this process is an important predictor of future GPP and trends in the
984 land-carbon sink. Nevertheless, this process remains largely unconsidered in regional and global climate model
985 simulations that are used to model carbon sources and sinks and carbon-climate feedbacks.

986

987

988

989 **Data availability**

990

991 The JULES model can be downloaded from the Met Office Science Repository Service
992 (<https://code.metoffice.gov.uk/trac/jules> - see here for a helpful how to [http://jules.jchmr.org/content/getting-](http://jules.jchmr.org/content/getting-started)
993 started). Model output data presented in this paper and the exact version of JULES with namelists are available
994 upon request from the corresponding author.

995

996 **Supplementary Information**

997

998 Supplementary_Information_Oliver_et_al.docx

999

1000 **Competing Interests**

1001 The authors declare that they have no conflict of interest

1002

1003 **Acknowledgements**

1004

1005 RJO and LMM were supported by the EU FP7 (ECLAIRE, 282910) and JWCRP (UKESM, NEC05816). This
1006 work was also supported by EMEP under UNECE. SS and LMM acknowledge the support of the NERC
1007 SAMBBA project (NE/J010057/1). The UK Met Office contribution was funded by BEIS under the Hadley Centre
1008 Climate Programme (GA01101). GAF also acknowledges funding from the EU's Horizon 2020 research and
1009 innovation programme (CRESCENDO, 641816). We also thank Magnus Engardt of SMHI for providing the
1010 RCA3 climate dataset. This work used eddy covariance data acquired and shared by the FLUXNET community,
1011 including these networks: AmeriFlux, AfriFlux, AsiaFlux, CarboAfrica, CarboEuropeIP, CarboItaly, CarboMont,

1012 ChinaFlux, Fluxnet-Canada, GreenGrass, ICOS, KoFlux, LBA, NECC, OzFlux-TERN, TCOS-Siberia, and
1013 USCCC. The ERA-Interim reanalysis data are provided by ECMWF and processed by LSCE. The FLUXNET
1014 eddy covariance data processing and harmonization was carried out by the European Fluxes Database Cluster,
1015 AmeriFlux Management Project, and Fluxdata project of FLUXNET, with the support of CDIAC and ICOS
1016 Ecosystem Thematic Center, and the OzFlux, ChinaFlux and AsiaFlux offices.

1017

1018

1019 **References**

1020

1021 Ainsworth, E., and Long, S.: What have we learned from 15 years of free-air CO₂ enrichment (FACE)?
1022 A meta-analytic review of the responses of photosynthesis, canopy properties and plant production
1023 to rising CO₂, *New Phytologist*, 165, 351-372, 2005.

1024 Ainsworth, E. A., Davey, P. A., Hymus, G. J., Osborne, C. P., Rogers, A., Blum, H., Nosberger, J., and
1025 Long, S. P.: Is stimulation of leaf photosynthesis by elevated carbon dioxide concentration
1026 maintained in the long term? A test with *Lolium perenne* grown for 10 years at two nitrogen
1027 fertilization levels under Free Air CO₂ Enrichment (FACE), *Plant, Cell and Environment*, 26, 705-714,
1028 2003.

1029 Ainsworth, E. A.: Rice production in a changing climate: a meta-analysis of responses to elevated
1030 carbon dioxide and elevated ozone concentration, *Global Change Biology*, 14, 1642-1650,
1031 10.1111/j.1365-2486.2008.01594.x, 2008.

1032 Ainsworth, E. A., Yendrek, C. R., Sitch, S., Collins, W. J., and Emberson, L. D.: The Effects of
1033 Tropospheric Ozone on Net Primary Productivity and Implications for Climate Change, *Annual
1034 Review of Plant Biology*, 63, 637-661, doi:10.1146/annurev-arplant-042110-103829, 2012.

1035 Anav, A., Menut, L., Khvorostyanov, D., and Viovy, N.: Impact of tropospheric ozone on the Euro-
1036 Mediterranean vegetation, *Global change biology*, 17, 2342-2359, 2011.

1037 Andersen, C. P.: Source-sink balance and carbon allocation below ground in plants exposed to
1038 ozone, *New Phytologist*, 157, 213-228, 10.1046/j.1469-8137.2003.00674.x, 2003.

1039 Arneeth, A., Harrison, S. P., Zaehle, S., Tsigaridis, K., Menon, S., Bartlein, P. J., Feichter, J., Korhola, A.,
1040 Kulmala, M., O'Donnell, D., Schurgers, G., Sorvari, S., and Vesala, T.: Terrestrial biogeochemical
1041 feedbacks in the climate system, *Nature Geosci*, 3, 525-532,
1042 http://www.nature.com/ngeo/journal/v3/n8/supinfo/ngeo905_S1.html, 2010.

1043 Avnery, S., Mauzerall, D. L., Liu, J., and Horowitz, L. W.: Global crop yield reductions due to surface
1044 ozone exposure: 1. Year 2000 crop production losses and economic damage, *Atmospheric
1045 Environment*, 45, 2284-2296, <https://doi.org/10.1016/j.atmosenv.2010.11.045>, 2011.

1046 Baig, S., Medlyn, B. E., Mercado, L. M., and Zaehle, S.: Does the growth response of woody plants to
1047 elevated CO₂ increase with temperature? A model-oriented meta-analysis, *Global Change Biology*,
1048 21, 4303-4319, 10.1111/gcb.12962, 2015.

1049 Bellamy, P. H., Loveland, P. J., Bradley, R. I., Lark, R. M., and Kirk, G. J.: Carbon losses from all soils
1050 across England and Wales 1978-2003, *Nature*, 437, 245-248, 2005.

1051 Bernacchi, C. J., Calfapietra, C., Davey, P. A., Wittig, V. E., Scarascia-Mugnozza, G. E., Raines, C. A.,
1052 and Long, S. P.: Photosynthesis and stomatal conductance responses of poplars to free-air CO₂
1053 enrichment (PopFACE) during the first growth cycle and immediately following coppice., *New
1054 Phytologist*, 159, 609-621, 2003.

1055 Best, M. J., Pryor, M., Clark, D. B., Rooney, G. G., Essery, R. L. H., Menard, C. B., Edwards, J. M.,
1056 Hendry, M. A., Porson, N., Gedney, N., Mercado, L. M., Sitch, S., Blyth, E., Boucher, O., Cox, P. M.,
1057 Grimmond, C. S. B., and Harding, R. J.: The Joint UK Land Environment Simulator (JULES), Model

1058 description - Part 1: Energy and water fluxes, Geoscientific Model Development Discussions, 4, 595-
1059 640, 10.5194/GMDD-4-595-2011, 2011.

1060 Betts, R. A., Boucher, O., Collins, M., Cox, P. M., Falloon, P. D., Gedney, N., Hemming, D. L.,
1061 Huntingford, C., Jones, C. D., and Sexton, D. M.: Projected increase in continental runoff due to plant
1062 responses to increasing carbon dioxide, *Nature*, 448, 1037-1041, 2007.

1063 Boden, T. A., Marland, G., and Andres, R. J.: Global, Regional, and National Fossil-Fuel CO₂ Emissions,
1064 Oak Ridge National Laboratory, U.S. Department of Energy, Oak Ridge, Tenn., USA, 2013.

1065 Büker, P., Feng, Z., Uddling, J., Briolat, A., Alonso, R., Braun, S., Elvira, S., Gerosa, G., Karlsson, P. E.,
1066 Le Thiec, D., Marzuoli, R., Mills, G., Oksanen, E., Wieser, G., Wilkinson, M., and Emberson, L. D.: New
1067 flux based dose-response relationships for ozone for European forest tree species, *Environmental*
1068 *Pollution*, 163-174, 2015.

1069 Calvete-Sogo, H., Elvira, S., Sanz, J., González-Fernández, I., García-Gómez, H., Sánchez-Martín, L.,
1070 Alonso, R., and Bermejo-Bermejo, V.: Current ozone levels threaten gross primary production and
1071 yield of Mediterranean annual pastures and nitrogen modulates the response, *Atmospheric*
1072 *Environment*, 95, 197-206, <http://dx.doi.org/10.1016/j.atmosenv.2014.05.073>, 2014.

1073 Capriel, P.: Trends in organic carbon and nitrogen contents in agricultural soils in Bavaria (south
1074 Germany) between 1986 and 2007, *European Journal of Soil Science*, 64, 445-454, 2013.

1075 Cech, P. G., Pepin, S., and Korner, C.: Elevated CO₂ reduces sap flux in mature deciduous forest trees,
1076 *Oecologia*, 137, 258-268, 2003.

1077 Ceulemans, R., and Mousseau, M.: Effects of elevated atmospheric CO₂ on woody plants, *New*
1078 *Phytologist*, 127, 1994.

1079 Ciais, P., Wattenbach, M., Vuichard, N., Smith, P., Piao, S., Don, A., Luyssaert, S., Janssens, I.,
1080 Bondeau, A., and Dechow, R.: The European carbon balance. Part 2: croplands, *Global Change*
1081 *Biology*, 16, 1409-1428, 2010.

1082 Ciais, P., Sabine, C., Bala, G., Bopp, L., Brovkin, V., Canadell, J., Chhabra, A., DeFries, R., Galloway, J.,
1083 Heimann, M., Jones, C., Le Quéré, C., Myneni, R. B., Piao, S., and Thornton, P.: Carbon and Other
1084 Biogeochemical Cycles. In: *Climate Change 2013: The Physical Science Basis. Contribution of Working*
1085 *Group I to the Fifth Assessment Report of the Intergovernmental Panel on Climate Change* [Stocker,
1086 T.F., D. Qin, G.-K. Plattner, M. Tignor, S.K. Allen, J. Boschung, A. Nauels, Y. Xia, V. Bex and P.M.
1087 Midgley (eds.)]. Cambridge University Press, Cambridge, United Kingdom and New York, NY, USA.,
1088 2013.

1089 Clark, D. B., Mercado, L. M., Sitch, S., Jones, C. D., Gedney, N., Best, M. J., Pryor, M., Rooney, G. G.,
1090 Essery, R. L. H., Blyth, E., Boucher, O., Harding, R. J., and Cox, P. M.: The Joint UK Land Environment
1091 Simulator (JULES), Model description - Part 2: Carbon fluxes and vegetation, *Geoscientific Model*
1092 *Development Discussions*, 4, 641-688, 10.5194/gmdd-4-641-2011, 2011.

1093 CLRTAP: The UNECE Convention on Long-range Transboundary Air Pollution. Manual on
1094 Methodologies and Criteria for Modelling and Mapping Critical Loads and Levels and Air Pollution
1095 Effects, Risks and Trends: Chapter III Mapping Critical Levels for Vegetation, accessed via,
1096 [http://icpvegetation.ceh.ac.uk/publications/documents/Chapter3-](http://icpvegetation.ceh.ac.uk/publications/documents/Chapter3-Mappingcriticallevelsforvegetation_000.pdf)
1097 [Mappingcriticallevelsforvegetation_000.pdf](http://icpvegetation.ceh.ac.uk/publications/documents/Chapter3-Mappingcriticallevelsforvegetation_000.pdf), 2017.

1098 Collins, W. J., Sitch, S., and Boucher, O.: How vegetation impacts affect climate metrics for ozone
1099 precursors, *Journal of Geophysical Research: Atmospheres*, 115, D23308, 10.1029/2010JD014187,
1100 2010.

1101 Collins, W. J., Bellouin, N., Doutriaux-Boucher, M., Gedney, N., Halloran, P., Hinton, T., Hughes, J.,
1102 Jones, C. D., Joshi, M., Liddicoat, S., Martin, G., O'Connor, F., Rae, J., Senior, C., Sitch, S., Totterdell, I.,
1103 Wiltshire, A., and Woodward, S.: Development and evaluation of an Earth-System model –
1104 HadGEM2, *Geosci. Model Dev.*, 4, 1051-1075, 10.5194/gmd-4-1051-2011, 2011.

1105 Cooper, O. R., Parrish, D. D., Stohl, A., Trainer, M., Nedelec, P., Thouret, V., Cammas, J. P., Oltmans,
1106 S. J., Johnson, B. J., Tarasick, D., Leblanc, T., McDermid, I. S., Jaffe, D., Gao, R., Stith, J., Ryerson, T.,
1107 Aikin, K., Campos, T., Weinheimer, A., and Avery, M. A.: Increasing springtime ozone mixing ratios in

1108 the free troposphere over western North America, *Nature*, 463, 344-348,
1109 http://www.nature.com/nature/journal/v463/n7279/supinfo/nature08708_S1.html, 2010.
1110 Cooper, O. R., Parrish, D., Ziemke, J., Balashov, N., Cupeiro, M., Galbally, I., Gilge, S., Horowitz, L.,
1111 Jensen, N., and Lamarque, J.-F.: Global distribution and trends of tropospheric ozone: An
1112 observation-based review, *Elementa: Science of the Anthropocene*, 2, 000029, 2014.
1113 Cox, P. M., Betts, R. A., Jones, C. D., Spall, S. A., and Totterdell, I. J.: Acceleration of global warming
1114 due to carbon-cycle feedbacks in a coupled climate model, *Nature*, 408, 184-187, 2000.
1115 Cox, P. M.: Description of the TRIFFID dynamic global vegetation model, Hadley Centre technical
1116 note 24, 2001.
1117 Cruz, F. T., Pitman, A. J., and Wang, Y. P.: Can the stomatal response to higher atmospheric carbon
1118 dioxide explain the unusual temperatures during the 2002 Murray-Darling Basin drought?, *Journal of*
1119 *Geophysical Research: Atmospheres*, 115, 2010.
1120 de Arellano, J. V.-G., van Heerwaarden, C. C., and Lelieveld, J.: Modelled suppression of boundary-
1121 layer clouds by plants in a CO₂-rich atmosphere, *Nature geoscience*, 5, 701-704, 2012.
1122 De Kauwe, M., Kala, J., Lin, Y.-S., Pitman, A., Medlyn, B., Duursma, R., Abramowitz, G., Wang, Y.-P.,
1123 and Miralles, D.: A test of an optimal stomatal conductance scheme within the CABLE land surface
1124 model, 8, 431-452, 2015.
1125 Derwent, R. G., Stevenson, D. S., Doherty, R. M., Collins, W. J., Sanderson, M. G., and Johnson, C. E.:
1126 Radiative forcing from surface NO_x emissions: spatial and seasonal variations, *Climatic Change*, 88,
1127 385-401, 10.1007/s10584-007-9383-8, 2008.
1128 Ellsworth, D. S.: CO₂ enrichment in a maturing pine forest: are CO₂ exchange and water status in the
1129 canopy affected?, *Plant, Cell and Environment*, 22, 461-472, 1999.
1130 Emberson, L. D., Ashmore, M. R., Cambridge, H. M., Simpson, D., and Tuovinen, J.-P.: Modelling
1131 stomatal ozone flux across Europe, *Environmental Pollution*, 109, 403-413, 2000.
1132 Emberson, L. D., Simpson, D., Tuovinen, J.-P., Ashmore, M. R., and Cambridge, H. M.: Modelling and
1133 mapping ozone deposition in Europe, *Water Air Soil Pollution*, 130, 577-582, 2001.
1134 Emberson, L. D., Büker, P., and Ashmore, M. R.: Assessing the risk caused by ground level ozone to
1135 European forest trees: A case study in pine, beech and oak across different climate regions,
1136 *Environmental Pollution*, 147, 454-466, 2007.
1137 Engardt, M., Simpson, D., Schwikowski, M., and Granat, L.: Deposition of sulphur and nitrogen in
1138 Europe 1900-2050. Model calculations and comparison to historical observations, *Tellus B: Chem.*
1139 *Phys. Meteor.*, 69, 2017.
1140 Etheridge, D. M., Steele, L. P., Langenfelds, R. L., Francey, R. J., M., B., and Morgan, V. I.: Natural and
1141 anthropogenic changes in atmospheric CO₂ over the last 1000 years from air in Antarctic ice and firn,
1142 *Journal of Geophysical Research*, 101(D2), 4115-4128, doi:10.1029/95JD03410, 1996.
1143 Fagnano, M., Maggio, A., and Fumagalli, I.: Crops' responses to ozone in Mediterranean
1144 environments, *Environmental Pollution*, 157, 1438-1444, 2009.
1145 Fares, S., Vargas, R., Detto, M., Goldstein, A. H., Karlik, J., Paoletti, E., and Vitale, M.: Tropospheric
1146 ozone reduces carbon assimilation in trees: estimates from analysis of continuous flux
1147 measurements, *Global change biology*, 19, 2427-2443, 2013.
1148 Felzer, B., Reilly, J., Melillo, J., Kicklighter, D., Sarofim, M., Wang, C., Prinn, R., and Zhuang, Q.: Future
1149 Effects of Ozone on Carbon Sequestration and Climate Change Policy Using a Global Biogeochemical
1150 Model, *Climatic Change*, 73, 345-373, 10.1007/s10584-005-6776-4, 2005.
1151 Felzer, B. S. F., Kicklighter, D. W., Melillo, J. M., Wang, C., Zhuang, Q., and Prinn, R. G.: Ozone effects
1152 on net primary productivity and carbon sequestration in the conterminous United States using a
1153 biogeochemistry model, *Tellus*, 56B, 230-248, 2004.
1154 Feng, Z., Kobayashi, K., and Ainsworth, E. A.: Impact of elevated ozone concentration on growth,
1155 physiology, and yield of wheat (*Triticum aestivum* L.): a meta-analysis, *Global Change Biology*, 14,
1156 2696-2708, 10.1111/j.1365-2486.2008.01673.x, 2008.

1157 Fowler, D., Flechard, C., Cape, J. N., Storeton-West, R. L., and Coyle, M.: Measurements of Ozone
1158 Deposition to Vegetation Quantifying the Flux, the Stomatal and Non-Stomatal Components, Water,
1159 Air, and Soil Pollution, 130, 63-74, 10.1023/a:1012243317471, 2001.

1160 Fowler, D., Pilegaard, K., Sutton, M., Ambus, P., Raivonen, M., Duyzer, J., Simpson, D., Fagerli, H.,
1161 Fuzzi, S., and Schjørring, J. K.: Atmospheric composition change: ecosystems–atmosphere
1162 interactions, Atmospheric Environment, 43, 5193-5267, 2009.

1163 Franz, M., Simpson, D., Arneth, A., and Zaehle, S.: Development and evaluation of an ozone
1164 deposition scheme for coupling to a terrestrial biosphere model, Biogeosciences, 14, 45-71,
1165 doi:10.5194/bg-14-45-2017, 2017.

1166 Friedlingstein, P., Cox, P., Betts, R., Bopp, L., von Bloh, W., Brovkin, V., Cadule, P., Doney, S., Eby, M.,
1167 Fung, I., Bala, G., John, J., Jones, C., Joos, F., Kato, T., Kawamiya, M., Knorr, W., Lindsay, K.,
1168 Matthews, H. D., Raddatz, T., Rayner, P., Reick, C., Roeckner, E., Schnitzler, K. G., Schnur, R.,
1169 Strassmann, K., Weaver, A. J., Yoshikawa, C., and Zeng, N.: Climate–Carbon Cycle Feedback Analysis:
1170 Results from the C4MIP Model Intercomparison, Journal of Climate, 19, 3337-3353,
1171 10.1175/jcli3800.1, 2006.

1172 Fuentes, J. D., Wang, D., Bowling, D. R., Potosnak, M., Monson, R. K., Goliff, W. S., and Stockwell, W.
1173 R.: Biogenic hydrocarbon chemistry within and above a mixed deciduous forest, Atmospheric
1174 Chemistry, 56, 165-185, 2007.

1175 Fuhrer, J., Val Martin, M., Mills, G., Heald, C. L., Harmens, H., Hayes, F., Sharps, K., Bender, J., and
1176 Ashmore, M. R.: Current and future ozone risks to global terrestrial biodiversity and ecosystem
1177 processes, Ecology and Evolution, 6, 8785-8799, 10.1002/ece3.2568, 2016.

1178 Garland, J. A., and Derwent, R. G.: Destruction at the ground and the diurnal cycle of concentration
1179 of ozone and other gases, Quarterly Journal of the Royal Meteorological Society, 105, 169-183,
1180 doi:10.1002/qj.49710544311, 1979.

1181 Gedney, N., Cox, P. M., Bett, R. A., Boucher, O., Huntingford, C., and Stott, P. A.: Detection of a direct
1182 carbon dioxide effect in continental river runoff records, Nature, 439, 835-838, 2006.

1183 Gerosa, G., Marzuoli, R., Monteleone, B., Chiesa, M., and Finco, A.: Vertical Ozone Gradients above
1184 Forests. Comparison of Different Calculation Options with Direct Ozone Measurements above a
1185 Mature Forest and Consequences for Ozone Risk Assessment, Forests, 8, 337, 2017.

1186 Grantz, D., Gunn, S., and VU, H. B.: O₃ impacts on plant development: a meta-analysis of root/shoot
1187 allocation and growth, Plant, cell & environment, 29, 1193-1209, 2006.

1188 Harmens, H., Mills, G., Emberson, L. D., and Ashmore, M. R.: Implications of climate change for the
1189 stomatal flux of ozone: A case study for winter wheat, Environmental Pollution, 146, 763-770,
1190 <http://dx.doi.org/10.1016/j.envpol.2006.05.018>, 2007.

1191 Hayes, F., Wagg, S., Mills, G., Wilkinson, S., and Davies, W.: Ozone effects in a drier climate:
1192 implications for stomatal fluxes of reduced stomatal sensitivity to soil drying in a typical grassland
1193 species, Global Change Biology, 18, 948-959, 2012.

1194 Heikkinen, J., Ketoja, E., Nuutinen, V., and Regina, K.: Declining trend of carbon in Finnish cropland
1195 soils in 1974–2009, Global Change Biology, 19, 1456-1469, 10.1111/gcb.12137, 2013.

1196 Hofmockel, K. S., Zak, D. R., Moran, K. K., and Jastrow, J. D.: Changes in forest soil organic matter
1197 pools after a decade of elevated CO₂ and O₃, Soil Biology and Biochemistry, 43, 1518-1527,
1198 <http://dx.doi.org/10.1016/j.soilbio.2011.03.030>, 2011.

1199 Hoshika, Y., Watanabe, M., Inada, N., and Koike, T.: Ozone-induced stomatal sluggishness develops
1200 progressively in Siebold's beech (*Fagus crenata*), Environmental Pollution, 166, 152-156, 2012a.

1201 Hoshika, Y., Omasa, K., and Paoletti, E.: Whole-Tree Water Use Efficiency Is Decreased by Ambient
1202 Ozone and Not Affected by O₃-Induced Stomatal Sluggishness, PLOS ONE, 7, e39270,
1203 10.1371/journal.pone.0039270, 2012b.

1204 Hoshika, Y., Watanabe, M., Inada, N., and Koike, T.: Model-based analysis of avoidance of ozone
1205 stress by stomatal closure in Siebold's beech (*Fagus crenata*), Annals of Botany, 112, 1149-1158,
1206 2013.

1207 Hoshika, Y., Katata, G., Deushi, M., Watanabe, M., Koike, T., and Paoletti, E.: Ozone-induced stomatal
1208 sluggishness changes carbon and water balance of temperate deciduous forests., *Scientific Reports*,
1209 doi:10.1038/srep09871, 2015.

1210 Hurtt, G., Chini, L. P., Frolking, S., Betts, R., Feddema, J., Fischer, G., Fisk, J., Hibbard, K., Houghton,
1211 R., Janetos, A., and Jones, C. D.: Harmonization of land-use scenarios for the period 1500–2100: 600
1212 years of global gridded annual land-use transitions, wood harvest, and resulting secondary lands,
1213 *Climatic Change*, 109, 117-161, 2011.

1214 IGBP-DIS: International Geosphere-Biosphere Programme, Data and Information System, Potsdam,
1215 Germany. Available from Oak Ridge National Laboratory Distributed Active Archive Center, Oak
1216 Ridge, TN, available at: <http://www.daac.ornl.gov>,

1217 IPCC: Climate change 2013: The Physical Science Basis, IPCC Working Group I Contribution to AR5,
1218 2013.

1219 Jacobs, C. M. J.: Direct impact of atmospheric CO₂ enrichment on regional transpiration, Wageningen
1220 Agricultural University, 1994.

1221 Janssens, I. A., Freibauer, A., Ciais, P., Smith, P., Nabuurs, G.-J., Folberth, G., Schlamadinger, B.,
1222 Hutjes, R. W. A., Ceulemans, R., Schulze, E.-D., Valentini, R., and Dolman, A. J.: Europe's Terrestrial
1223 Biosphere Absorbs 7 to 12% of European Anthropogenic CO₂ Emissions, *Science*, 300, 1538-1542,
1224 10.1126/science.1083592, 2003.

1225 Jones, C. D., Cox, P., and Huntingford, C.: Uncertainty in climate–carbon-cycle projections associated
1226 with the sensitivity of soil respiration to temperature, *Tellus B*, 55, 642-648, 10.1034/j.1600-
1227 0889.2003.01440.x, 2003.

1228 Jung, M., Reichstein, M., Margolis, H. A., Cescatti, A., Richardson, A. D., Arain, M. A., Arneth, A.,
1229 Bernhofer, C., Bonal, D., Chen, J., Gianelle, D., Gobron, N., Kiely, G., Kutsch, W., Lasslop, G., Law, B.
1230 E., Lindroth, A., Merbold, L., Montagnani, L., Moors, E. J., Papale, D., Sottocornola, M., Vaccari, F.,
1231 and Williams, C.: Global patterns of land-atmosphere fluxes of carbon dioxide, latent heat, and
1232 sensible heat derived from eddy covariance, satellite, and meteorological observations, *Journal of*
1233 *Geophysical Research: Biogeosciences*, 116, n/a-n/a, 10.1029/2010JG001566, 2011.

1234 Kala, J., De Kauwe, M. G., Pitman, A. J., Medlyn, B. E., Wang, Y. P., Lorenz, R., and Perkins-Kirkpatrick,
1235 S. E.: Impact of the representation of stomatal conductance on model projections of heatwave
1236 intensity., *Scientific Reports*, 1-7, 10.1038/srep23418, 2016.

1237 Karlsson, P., Hansson, M., Höglund, H. O., and Pleijel, H.: Ozone concentration gradients and wind
1238 conditions in Norway spruce (*Picea abies*) forests in Sweden, *Atmospheric Environment*, 1610-1618
1239 pp., 2006.

1240 Karlsson, P. E., Braun, S., Broadmeadow, M., Elvira, S., Emberson, L., Gimeno, B. S., Le Thiec, D.,
1241 Novak, K., Oksanen, E., Schaub, M., Uddling, J., and Wilkinson, M.: Risk assessments for forest trees:
1242 The performance of the ozone flux versus the AOT concepts, *Environmental Pollution*, 146, 608-616,
1243 <http://dx.doi.org/10.1016/j.envpol.2006.06.012>, 2007.

1244 Karnosky, D., Percy, K. E., Xiang, B., Callan, B., Noormets, A., Mankovska, B., Hopkin, A., Sober, J.,
1245 Jones, W., and Dickson, R.: Interacting elevated CO₂ and tropospheric O₃ predisposes aspen
1246 (*Populus tremuloides* Michx.) to infection by rust (*Melampsora medusae* f. sp. *tremuloidae*), *Global*
1247 *Change Biology*, 8, 329-338, 2002.

1248 Karnosky, D. F., Skelly, J. M., Percy, K. E., and Chappelka, A. H.: Perspectives regarding 50years of
1249 research on effects of tropospheric ozone air pollution on US forests, *Environmental Pollution*, 147,
1250 489-506, 2007.

1251 Keeling, C. D., and Whorf, T. P.: Atmospheric CO₂ records from sites in the SIO air sampling network.
1252 In *Trends: A Compendium of Data on Global Change*, Carbon Dioxide Information Analysis Center,
1253 Oak Ridge National Laboratory, Oak Ridge, Tenn., U.S.A. , 2004.

1254 Kitao, M., Löw, M., Heerdt, C., Grams, T. E., Häberle, K.-H., and Matyssek, R.: Effects of chronic
1255 elevated ozone exposure on gas exchange responses of adult beech trees (*Fagus sylvatica*) as related
1256 to the within-canopy light gradient, *Environmental Pollution*, 157, 537-544, 2009.

1257 Kjellström, E., Nikulin, G., Hansson, U., Strandberg, G., and Ullerstig, A.: 21st century changes in the
1258 European climate: uncertainties derived from an ensemble of regional climate model simulations,
1259 *Tellus A*, 63, 24-40, 2011.

1260 Kubiske, M., Quinn, V., Marquardt, P., and Karnosky, D.: Effects of Elevated Atmospheric CO₂ and/or
1261 O₃ on Intra-and Interspecific Competitive Ability of Aspen, *Plant biology*, 9, 342-355, 2007.

1262 Lamarque, J., Shindell, D. T., Josse, B., Young, P., Cionni, I., Eyring, V., Bergmann, D., Cameron-Smith,
1263 P., Collins, W. J., and Doherty, R.: The Atmospheric Chemistry and Climate Model Intercomparison
1264 Project (ACCMIP): overview and description of models, simulations and climate diagnostics,
1265 *Geoscientific Model Development*, 6, 179-206, 2013.

1266 Langner, J., Engardt, M., Baklanov, A., Christensen, J. H., Gauss, M., Geels, C., Hedegaard, G. B.,
1267 Nuterman, R., Simpson, D., and Soares, J.: A multi-model study of impacts of climate change on
1268 surface ozone in Europe, *Atmospheric Chemistry and Physics*, 12, 10423-10440, 2012a.

1269 Langner, J., Engardt, M., and Andersson, C.: European summer surface ozone 1990–2100,
1270 *Atmospheric Chemistry and Physics*, 12, 10097-10105, 2012b.

1271 Le Quéré, C., Moriarty, R., Andrew, R. M., Peters, G. P., Ciais, P., Friedlingstein, P., Jones, S. D., Sitch,
1272 S., Tans, P., Arneeth, A., Boden, T. A., Bopp, L., Bozec, Y., Canadell, J. G., Chini, L. P., Chevallier, F.,
1273 Cosca, C. E., Harris, I., Hoppema, M., Houghton, R. A., House, J. I., Jain, A. K., Johannessen, T., Kato,
1274 E., Keeling, R. F., Kitidis, V., Klein Goldewijk, K., Koven, C., Landa, C. S., Landschützer, P., Lenton, A.,
1275 Lima, I. D., Marland, G., Mathis, J. T., Metz, N., Nojiri, Y., Olsen, A., Ono, T., Peng, S., Peters, W., Pfeil,
1276 B., Poulter, B., Raupach, M. R., Regnier, P., Rödenbeck, C., Saito, S., Salisbury, J. E., Schuster, U.,
1277 Schwinger, J., Séférian, R., Segschneider, J., Steinhoff, T., Stocker, B. D., Sutton, A. J., Takahashi, T.,
1278 Tilbrook, B., van der Werf, G. R., Viovy, N., Wang, Y. P., Wanninkhof, R., Wiltshire, A., and Zeng, N.:
1279 Global carbon budget 2014, *Earth Syst. Sci. Data*, 7, 47-85, 10.5194/essd-7-47-2015, 2015.

1280 Le Quéré, C., Andrew, R. M., Canadell, J. G., Sitch, S., Korsbakken, J. I., Peters, G. P., Manning, A. C.,
1281 Boden, T. A., Tans, P. P., Houghton, R. A., Keeling, R. F., Alin, S., Andrews, O. D., Anthoni, P., Barbero,
1282 L., Bopp, L., Chevallier, F., Chini, L. P., Ciais, P., Currie, K., Delire, C., Doney, S. C., Friedlingstein, P.,
1283 Gkritzalis, T., Harris, I., Hauck, J., Haverd, V., Hoppema, M., Klein Goldewijk, K., Jain, A. K., Kato, E.,
1284 Körtzinger, A., Landschützer, P., Lefèvre, N., Lenton, A., Lienert, S., Lombardozzi, D., Melton, J. R.,
1285 Metz, N., Millero, F., Monteiro, P. M. S., Munro, D. R., Nabel, J. E. M. S., Nakaoka, S. I., O'Brien, K.,
1286 Olsen, A., Omar, A. M., Ono, T., Pierrot, D., Poulter, B., Rödenbeck, C., Salisbury, J., Schuster, U.,
1287 Schwinger, J., Séférian, R., Skjelvan, I., Stocker, B. D., Sutton, A. J., Takahashi, T., Tian, H., Tilbrook, B.,
1288 van der Laan-Luijckx, I. T., van der Werf, G. R., Viovy, N., Walker, A. P., Wiltshire, A. J., and Zaehle, S.:
1289 Global Carbon Budget 2016, *Earth Syst. Sci. Data*, 8, 605-649, 10.5194/essd-8-605-2016, 2016.

1290 Le Quéré, C., Andrew, R. M., Friedlingstein, P., Sitch, S., Pongratz, J., Manning, A. C., Korsbakken, J. I.,
1291 Peters, G. P., Canadell, J. G., Jackson, R. B., Boden, T. A., Tans, P. P., Andrews, O. D., Arora, V. K.,
1292 Bakker, D. C. E., Barbero, L., Becker, M., Betts, R. A., Bopp, L., Chevallier, F., Chini, L. P., Ciais, P.,
1293 Cosca, C. E., Cross, J., Currie, K., Gasser, T., Harris, I., Hauck, J., Haverd, V., Houghton, R. A., Hunt, C.
1294 W., Hurtt, G., Ilyina, T., Jain, A. K., Kato, E., Kautz, M., Keeling, R. F., Klein Goldewijk, K., Körtzinger,
1295 A., Landschützer, P., Lefèvre, N., Lenton, A., Lienert, S., Lima, I., Lombardozzi, D., Metz, N., Millero,
1296 F., Monteiro, P. M. S., Munro, D. R., Nabel, J. E. M. S., Nakaoka, S.-I., Nojiri, Y., Padín, X. A., Pregon,
1297 A., Pfeil, B., Pierrot, D., Poulter, B., Rehder, G., Reimer, J., Rödenbeck, C., Schwinger, J., Séférian, R.,
1298 Skjelvan, I., Stocker, B. D., Tian, H., Tilbrook, B., van der Laan-Luijckx, I. T., van der Werf, G. R., van
1299 Heuven, S., Viovy, N., Vuichard, N., Walker, A. P., Watson, A. J., Wiltshire, A. J., Zaehle, S., and Zhu,
1300 D.: Global Carbon Budget 2017, *Earth Syst. Sci. Data Discuss*, in review, 2017.

1301 Leuzinger, S., and Körner, C.: Water savings in mature deciduous forest trees under elevated CO₂,
1302 *Global Change Biology*, 13, 2498-2508, doi:10.1111/j.1365-2486.2007.01467.x, 2007.

1303 Lin, Y.-S., Medlyn, B. E., Duursma, R. A., Prentice, I. C., Wang, H., Baig, S., Eamus, D., de Dios, V. R.,
1304 Mitchell, P., and Ellsworth, D. S.: Optimal stomatal behaviour around the world, *Nature Climate
1305 Change*, 5, 459-464, 2015.

1306 Lindroth, R. L.: Impacts of Elevated Atmospheric CO₂ and O₃ on Forests: Phytochemistry, Trophic
1307 Interactions, and Ecosystem Dynamics, *Journal of Chemical Ecology*, 36, 2-21, 10.1007/s10886-009-
1308 9731-4, 2010.

1309 Logan, J. A., Staehelin, J., Megretskaia, I. A., Cammas, J. P., Thouret, V., Claude, H., De Backer, H.,
1310 Steinbacher, M., Scheel, H. E., Stübi, R., Fröhlich, M., and Derwent, R.: Changes in ozone over
1311 Europe: Analysis of ozone measurements from sondes, regular aircraft (MOZAIC) and alpine surface
1312 sites, *Journal of Geophysical Research*, 117, 1-23, 2012.

1313 Lombardozzi, D., Levis, S., Bonan, G., and Sparks, J. P.: Predicting photosynthesis and transpiration
1314 responses to ozone: decoupling modeled photosynthesis and stomatal conductance, *Biogeosciences*,
1315 3113-3130, 2012.

1316 Lombardozzi, D., Levis, S., Bonan, G., Hess, P. G., and Sparks, J. P.: The Influence of Chronic Ozone
1317 Exposure on Global Carbon and Water Cycles, *Journal of Climate*, 28, 292-305, 10.1175/jcli-d-14-
1318 00223.1, 2015.

1319 Long, S. P., Ainsworth, E. A., Leakey, A. D. B., Nosberger, J., and Ort, D. R.: Food for Thought: Lower-
1320 Than-Expected Crop Yield Stimulation with Rising CO₂ Concentrations, *Science*, 312, 1918-1921,
1321 10.1126/science.1114722, 2006.

1322 Löw, M., Herbinger, K., Nunn, A., Häberle, K.-H., Leuchner, M., Heerdt, C., Werner, H., Wipfler, P.,
1323 Pretzsch, H., and Tausz, M.: Extraordinary drought of 2003 overrules ozone impact on adult beech
1324 trees (*Fagus sylvatica*), *Trees*, 20, 539-548, 2006.

1325 Loya, W. M., Pregitzer, K. S., Karberg, N. J., King, J. S., and Giardina, C. P.: Reduction of soil carbon
1326 formation by tropospheric ozone under increased carbon dioxide levels., *Nature*, 425, 705-707,
1327 2003.

1328 Luyssaert, S., Abril, G., Andres, R., Bastviken, D., Bellassen, V., Bergamaschi, P., Bousquet, P.,
1329 Chevallier, F., Ciais, P., Corazza, M., Dechow, R., Erb, K. H., Etiope, G., Fortems-Cheiney, A., Grassi, G.,
1330 Hartmann, J., Jung, M., Lathière, J., Lohila, A., Mayorga, E., Moosdorf, N., Njakou, D. S., Otto, J.,
1331 Papale, D., Peters, W., Peylin, P., Raymond, P., Rödenbeck, C., Saarnio, S., Schulze, E. D., Szopa, S.,
1332 Thompson, R., Verkerk, P. J., Vuichard, N., Wang, R., Wattenbach, M., and Zaehle, S.: The European
1333 land and inland water CO₂, CO, CH₄ and N₂O balance between 2001 and 2005, *Biogeosciences*, 9,
1334 3357-3380, 10.5194/bg-9-3357-2012, 2012.

1335 Massman, W. J.: A review of the molecular diffusivities of H₂O, CO₂, CH₄, CO, O₃, SO₂, NH₃, N₂O,
1336 NO, and NO₂ in air, O₂ and N₂ near STP, *Atmospheric Environment*, 32, 1111-1127,
1337 [http://dx.doi.org/10.1016/S1352-2310\(97\)00391-9](http://dx.doi.org/10.1016/S1352-2310(97)00391-9), 1998.

1338 Matyssek, R., Wieser, G., Ceulemans, R., Rennenberg, H., Pretzsch, H., Haberer, K., Löw, M., Nunn,
1339 A., Werner, H., and Wipfler, P.: Enhanced ozone strongly reduces carbon sink strength of adult beech
1340 (*Fagus sylvatica*)—Resume from the free-air fumigation study at Kranzberg Forest, *Environmental*
1341 *Pollution*, 158, 2527-2532, 2010a.

1342 Matyssek, R., Karnosky, D., Wieser, G., Percy, K., Oksanen, E., Grams, T., Kubiske, M., Hanke, D., and
1343 Pretzsch, H.: Advances in understanding ozone impact on forest trees: messages from novel
1344 phytotron and free-air fumigation studies, *Environmental Pollution*, 158, 1990-2006, 2010b.

1345 McLaughlin, S. B., Nosal, M., Wullschleger, S. D., and Sun, G.: Interactive effects of ozone and climate
1346 on tree growth and water use in a southern Appalachian forest in the USA, *New Phytologist*, 174,
1347 109-124, 10.1111/j.1469-8137.2007.02018.x, 2007a.

1348 McLaughlin, S. B., Wullschleger, S. D., Sun, G., and Nosal, M.: Interactive effects of ozone and climate
1349 on water use, soil moisture content and streamflow in a southern Appalachian forest in the USA,
1350 *New Phytologist*, 174, 125-136, 10.1111/j.1469-8137.2007.01970.x, 2007b.

1351 Medlyn, B. E., Badeck, F. W., De Pury, D. G. G., Barton, C. V. M., Broadmeadow, M., Ceulemans, R.,
1352 De Angelis, P., Forstreuter, M., Jach, M. E., Kellomaki, S., Laitat, E., Marek, M., Philippot, S., Rey, A.,
1353 Strassmeyer, J., Laitinen, K., Liozon, R., Portier, B., Roberntz, P., Wang, K., and Jstbid, P. G.: Effects
1354 of elevated [CO₂] on photosynthesis in European forest species: a meta-analysis of model
1355 parameters, *Plant, Cell & Environment*, 22, 1475-1495, doi:10.1046/j.1365-3040.1999.00523.x, 1999.

1356 Medlyn, B. E., Barton, C. V. M., Broadmeadow, M. S. J., Ceulemans, R., De Angelis, P., Forstreuter,
1357 M., Freeman, M., Jackson, S. B., Kellomaki, S., Laitat, E., Rey, A., Roberntz, P., Sigurdsson, B. D.,
1358 Strassmeyer, J., Wang, K., Curtis, P. S., and Jarvis, P. G.: Stomatal conductance of forest species
1359 after long-term exposure to elevated CO₂ concentration: a synthesis, *New Phytologist*, 149, 247-264,
1360 2001.

1361 Medlyn, B. E., Duursma, R. A., Eamus, D., Ellsworth, D. S., Prentice, I. C., Barton, C. V., Crous, K. Y., de
1362 Angelis, P., Freeman, M., and Wingate, L.: Reconciling the optimal and empirical approaches to
1363 modelling stomatal conductance, *Global Change Biology*, 17, 2134-2144, 2011.

1364 Mercado, L. M., Bellouin, N., Sitch, S., Boucher, O., Huntingford, C., Wild, M., and Cox, P. M.: Impact
1365 of changes in diffuse radiation on the global land carbon sink, *Nature*, 458, 1014-1017,
1366 http://www.nature.com/nature/journal/v458/n7241/supinfo/nature07949_S1.html, 2009.

1367 Mills, G., Hayes, F., Wilkinson, S., and Davies, W. J.: Chronic exposure to increasing background
1368 ozone impairs stomatal functioning in grassland species, *Global Change Biology*, 15, 1522-1533,
1369 2009.

1370 Mills, G., Pleijel, H., Braun, S., Büker, P., Bermejo, V., Calvo, E., Danielsson, H., Emberson, L.,
1371 Grünhage, L., Fernández, I. G., Harmens, H., Hayes, F., Karlsson, P.-E., and Simpson, D.: New stomatal
1372 flux-based critical levels for ozone effects on vegetation, *Atmospheric Environment*, 5064-5068,
1373 2011a.

1374 Mills, G., Hayes, F., Simpson, D., Emberson, L., Norris, D., Harmens, H., and BÜKER, P.: Evidence of
1375 widespread effects of ozone on crops and (semi-)natural vegetation in Europe (1990–2006) in
1376 relation to AOT40- and flux-based risk maps, *Global Change Biology*, 17, 592-613, 10.1111/j.1365-
1377 2486.2010.02217.x, 2011b.

1378 Mills, G., Harmens, H., Wagg, S., Sharps, K., Hayes, F., Fowler, D., Sutton, M., and Davies, B.: Ozone
1379 impacts on vegetation in a nitrogen enriched and changing climate, *Environmental Pollution*, 208,
1380 898-908, 2016.

1381 Norby, R. J., Wullschlegel, S. D., Gunderson, C. A., Johnson, D. W., and Ceulemans, R.: Tree responses
1382 to rising CO₂ in field experiments: implications for the future forest, *Plant, Cell and Environment*, 22,
1383 683-714, 1999.

1384 Norby, R. J., DeLucia, E. H., Gielen, B., Calfapietra, C., Giardina, C. P., King, J. S., Ledford, J., McCarthy,
1385 H. R., Moore, D. J. P., Ceulemans, R., De Angelis, P., Finzi, A. C., Karnosky, D. F., Kubiske, M. E., Lukac,
1386 M., Pregitzer, K. S., Scarascia-Mugnozza, G. E., Schlesinger, W. H., and Oren, R.: Forest response to
1387 elevated CO₂ is conserved across a broad range of productivity, *Proc. Natl. Acad. Sci. U. S. A.*, 102,
1388 18052-18056, 10.1073/pnas.0509478102, 2005.

1389 Nunn, A. J., Reiter, I. M., Häberle, K.-H., Langebartels, C., Bahnweg, G., Pretzsch, H., Sandermann, H.,
1390 and Matyssek, R.: Response patterns in adult forest trees to chronic ozone stress: identification of
1391 variations and consistencies, *Environmental Pollution*, 136, 365-369, 2005.

1392 O'Connor, F. M., Johnson, C. E., Morgenstern, O., Abraham, N. L., Braesicke, P., Dalvi, M., Folberth,
1393 G. A., Sanderson, M. G., Telford, P. J., Voulgarakis, A., Young, P. J., Zeng, G., Collins, W. J., and Pyle, J.
1394 A.: Evaluation of the new UKCA climate-composition model – Part 2: The Troposphere, *Geosci.*
1395 *Model Dev.*, 7, 41-91, 10.5194/gmd-7-41-2014, 2014.

1396 Paoletti, E., and Grulke, N. E.: Ozone exposure and stomatal sluggishness in different plant
1397 physiognomic classes, *Environmental Pollution*, 158, 2664-2671, 2010.

1398 Parrish, D. D., Law, K. S., Staehelin, J., Derwent, R., Cooper, O. R., Tanimoto, H., Volz-Thomas, A.,
1399 Gilge, S., Scheel, H. E., Steinbacher, M., and Chan, E.: Long-term changes in lower tropospheric
1400 baseline ozone concentrations at northern mid-latitudes, *Atmos. Chem. Phys.*, 12, 11485-11504,
1401 10.5194/acp-12-11485-2012, 2012.

1402 Parrish, D. D., Law, K. S., Staehelin, J., Derwent, R., Cooper, O. R., Tanimoto, H., Volz-Thomas, A.,
1403 Gilge, S., Scheel, H. E., Steinbacher, M., and Chan, E.: Lower tropospheric ozone at northern
1404 midlatitudes: Changing seasonal cycle, *Geophysical Research Letters*, 40, 1631-1636, 2013.

1405 Percy, K. E., Awmack, C. S., Lindroth, R. L., Kubiske, M. E., Kopper, B. J., Isebrands, J., Pregitzer, K. S.,
1406 Hendrey, G. R., Dickson, R. E., and Zak, D. R.: Altered performance of forest pests under atmospheres
1407 enriched by CO₂ and O₃, *Nature*, 420, 403-407, 2002.

1408 Royal-Society: Ground-level ozone in the 21st century: future trends, impacts and policy
1409 implications, *Science Policy Report 15/08*, 2008.

1410 Samuelsson, P., Jones, C. G., Willén, U., Ullerstig, A., Gollvik, S., Hansson, U., Jansson, C., Kjellström,
1411 E., Nikulin, G., and Wyser, K.: The Rossby Centre Regional Climate model RCA3: model description
1412 and performance, *Tellus A*, 63, 4-23, 2011.

1413 Saxe, H., Ellsworth, D. S., and Heath, J.: Tree and forest functioning in an enriched CO₂ atmosphere,
1414 *New Phytologist*, 139, 395-436, doi:10.1046/j.1469-8137.1998.00221.x, 1998.

1415 Schulze, E.-D., Ciais, P., Luysaert, S., Schruppf, M., Janssens, I. A., Thiruchittampalam, B., Theloke, J.,
1416 Saurat, M., Bringezu, S., and Lelieveld, J.: The European carbon balance. Part 4: integration of carbon
1417 and other trace-gas fluxes, *Global Change Biology*, 16, 1451-1469, 2010.

1418 Schulze, E. D., Luysaert, S., Ciais, P., Freibauer, A., Janssens, I. A., and et al.: Importance of methane
1419 and nitrous oxide for Europe's terrestrial greenhouse-gas balance, *Nature Geosci*, 2, 842-850,
1420 http://www.nature.com/ngeo/journal/v2/n12/supinfo/ngeo686_S1.html, 2009.

1421 Sicard, P., De Marco, A., Troussier, F., Renoua, C., Vas, N., and Paoletti, E.: Decrease in surface ozone
1422 concentrations at Mediterranean remote sites and increase in the cities, *Atmospheric Environment*,
1423 79, 705-715, 2013.

1424 Simpson, D., Emberson, L., Ashmore, M., and Tuovinen, J.: A comparison of two different approaches
1425 for mapping potential ozone damage to vegetation. A model study *Environmental Pollution*, 146,
1426 715-725, 2007.

1427 Simpson, D., Benedictow, A., Berge, H., Bergström, R., Emberson, L. D., Fagerli, H., Flechard, C. R.,
1428 Hayman, G. D., Gauss, M., and Jonson, J. E.: The EMEP MSC-W chemical transport model—technical
1429 description, *Atmospheric Chemistry and Physics*, 12, 7825-7865, 2012.

1430 Simpson, D., Andersson, C., Christensen, J. H., Engardt, M., Geels, C., Nyiri, A., Posch, M., Soares, J.,
1431 Sofiev, M., and Wind, P.: Impacts of climate and emission changes on nitrogen deposition in Europe:
1432 a multi-model study, *Atmospheric Chemistry and Physics*, 14, 6995-7017, 2014a.

1433 Simpson, D., Arneth, A., Mills, G., Solberg, S., and Uddling, J.: Ozone—the persistent menace:
1434 interactions with the N cycle and climate change, *Current Opinion in Environmental Sustainability*, 9,
1435 9-19, 2014b.

1436 Sitch, S., Cox, P. M., Collins, W. J., and Huntingford, C.: Indirect radiative forcing of climate change
1437 through ozone effects on the land-carbon sink, *Nature*, 448, 791-794,
1438 http://www.nature.com/nature/journal/v448/n7155/supinfo/nature06059_S1.html, 2007.

1439 Sitch, S., Friedlingstein, P., Gruber, N., Jones, S. D., Murray-Tortarolo, G., Ahlström, A., Doney, S. C.,
1440 Graven, H., Heinze, C., Huntingford, C., Levis, S., Levy, P. E., Lomas, M., Poulter, B., Viovy, N., Zaehle,
1441 S., Zeng, N., Arneth, A., Bonan, G., Bopp, L., Canadell, J. G., Chevallier, F., Ciais, P., Ellis, R., Gloor, M.,
1442 Peylin, P., Piao, S. L., Le Quéré, C., Smith, B., Zhu, Z., and Myneni, R.: Recent trends and drivers of
1443 regional sources and sinks of carbon dioxide, *Biogeosciences*, 12, 653-679, 10.5194/bg-12-653-2015,
1444 2015.

1445 Sleutel, S., De Neve, S., and Hofman, G.: Estimates of carbon stock changes in Belgian cropland., *Soil
1446 Use and Management*, 19, 166-171, 10.1079/SUM2003187, 2003.

1447 Sun, G. E., McLaughlin, S. B., Porter, J. H., Uddling, J., Mulholland, P. J., Adams, M. B., and Pederson,
1448 N.: Interactive influences of ozone and climate on streamflow of forested watersheds, *Global Change
1449 Biology*, 18, 3395-3409, 10.1111/j.1365-2486.2012.02787.x, 2012.

1450 Tai, P. K. A., Val Martin, M., and Heald, C. L.: Threat to future global food security from climate
1451 change and ozone air pollution, *Nature Climate Change*, 4, 817 - 821, 2014.

1452 Talhelm, A. F., Pregitzer, K. S., Kubiske, M. E., Zak, D. R., Company, C. E., Burton, A. J., Dickson, R. E.,
1453 Hendrey, G. R., Isebrands, J. G., Lewin, K. F., Nagy, J., and Karnosky, D. F.: Elevated carbon dioxide
1454 and ozone alter productivity and ecosystem carbon content in northern temperate forests, *Global
1455 Change Biology*, 20, 2492-2504, 10.1111/gcb.12564, 2014.

1456 Tans, P., and Keeling, R.: Dr. Pieter Tans, NOAA/ESRL (www.esrl.noaa.gov/gmd/ccgg/trends/) and Dr.
1457 Ralph Keeling, Scripps Institution of Oceanography (scrippsco2.ucsd.edu/).
1458 Tricker, P. J., Pecchiari, M., Bunn, S. M., Vaccari, F. P., Peressotti, A., Miglietta, F., and Taylor, G.:
1459 Water use of a bioenergy plantation increases in a future high CO₂ world, *Biomass and Bioenergy*,
1460 33, 200-208, 2009.
1461 Tuovinen, J.-P., Emberson, L., and Simpson, D.: Modelling ozone fluxes to forests for risk assessment:
1462 status and prospects, *Annals of Forest Science*, 66, 1-14, 2009.
1463 Tuovinen, J., Hakola, H., Karlsson, P., and Simpson, D.: Air pollution risks to Northern European
1464 forests in a changing climate, *Climate Change, Air Pollution and Global Challenges Understanding*
1465 *and Perspectives from Forest Research*, 2013.
1466 Uddling, J., Teclaw, R. M., Pregitzer, K. S., and Ellsworth, D. S.: Leaf and canopy conductance in aspen
1467 and aspen-birch forests under free-air enrichment of carbon dioxide and ozone, *Tree Physiology*, 29,
1468 1367-1380, 2009.
1469 Val Martin, M., Heald, C. L., and Arnold, S. R.: Coupling dry deposition to vegetation phenology in the
1470 Community Earth System Model: Implications for the simulation of surface O₃, *Geophysical*
1471 *Research Letters*, 41, 2988-2996, doi:10.1002/2014GL059651, 2014.
1472 van Vuuren, D. P., Edmonds, J., Kainuma, M., Riahi, K., Thomson, A., Hibbard, K., Hurtt, G. C., Kram,
1473 T., Krey, V., Lamarque, J.-F., Masui, T., Meinshausen, M., Nakicenovic, N., Smith, S. J., and Rose, S. K.:
1474 The representative concentration pathways: an overview, *Climatic Change*, 109, 5, 10.1007/s10584-
1475 011-0148-z, 2011.
1476 Verstraeten, W. W., Neu, J. L., Williams, J. E., Bowman, K. W., Worden, J. R., and Boersma, K. F.:
1477 Rapid increases in tropospheric ozone production and export from China, *Nature Geoscience* 8, 690-
1478 695, 2015.
1479 Vingarzan, R.: A review of surface ozone background levels and trends, *Atmospheric Environment*,
1480 38, 3431-3442, <https://doi.org/10.1016/j.atmosenv.2004.03.030>, 2004.
1481 Weedon, G. P., Gomes, S., Viterbo, P., Österle, H., Adam, J. C., Bellouin, N., Boucher, O., and Best, M.
1482 J.: The WATCH Forcing Data 1958-2001: a meteorological forcing dataset for land surface- and
1483 hydrological models. , WATCH Tech. Rep. 22, 41p (available at www.eu-watch.org/publications).
1484 2010.
1485 Weedon, G. P., Gomes, S., Viterbo, P., Shuttleworth, W. J., Blyth, E., Österle, H., Adam, J. C., Bellouin,
1486 N., Boucher, O., and Best, M.: Creation of the WATCH Forcing data and its use to assess global and
1487 regional reference crop evaporation over land during the twentieth century, *Journal of*
1488 *Hydrometeorology*, 12, 823-848, doi: 10.1175/2011JHM1369.1., 2011.
1489 Weedon, G. P.: Readme file for the "WFDEI" dataset.available at: [http://www.eu-](http://www.eu-watch.org/gfx_content/documents/README-WFDEI.pdf)
1490 [watch.org/gfx_content/documents/README-WFDEI.pdf](http://www.eu-watch.org/gfx_content/documents/README-WFDEI.pdf), 2013.
1491 Wild, O.: Modelling the global tropospheric ozone budget: exploring the
1492 variability in current models, *Atmospheric Chemistry and Physics*, 2643-2660, 2007.
1493 Wilkinson, S., and Davies, W. J.: Ozone suppresses soil drying-and abscisic acid (ABA)-induced
1494 stomatal closure via an ethylene-dependent mechanism, *Plant, Cell & Environment*, 32, 949-959,
1495 2009.
1496 Wilkinson, S., and Davies, W. J.: Drought, ozone, ABA and ethylene: new insights from cell to plant to
1497 community, *Plant, Cell & Environment*, 33, 510-525, 10.1111/j.1365-3040.2009.02052.x, 2010.
1498 Wittig, V. E., Ainsworth, E. A., and Long, S. P.: To what extent do current and projected increases in
1499 surface ozone affect photosynthesis and stomatal conductance of trees? A meta-analytic review of
1500 the last 3 decades of experiments, *Plant, Cell & Environment*, 30, 1150-1162, 10.1111/j.1365-
1501 3040.2007.01717.x, 2007.
1502 Wittig, V. E., Ainsworth, E. A., Naidu, S. L., Karnosky, D. F., and Long, S. P.: Quantifying the impact of
1503 current and future tropospheric ozone on tree biomass, growth, physiology and biochemistry: a
1504 quantitative meta-analysis, *Global Change Biology*, 15, 396-424, 10.1111/j.1365-2486.2008.01774.x,
1505 2009.

1506 Wullschleger, S. D., Gunderson, C. A., Hanson, P. J., Wilson, K. B., and Norby, R. J.: Sensitivity of
1507 stomatal and canopy conductance to elevated CO₂ concentration; interacting variables and
1508 perspectives of scale, *New Phytologist*, 153, 485-496, doi:10.1046/j.0028-646X.2001.00333.x, 2002.
1509 Young, P., Arneth, A., Schurgers, G., Zeng, G., and Pyle, J. A.: The CO₂ inhibition of terrestrial isoprene
1510 emission significantly affects future ozone projections, *Atmospheric Chemistry and Physics*, 9, 2793-
1511 2803, 2009.
1512 Young, P., Archibald, A., Bowman, K., Lamarque, J.-F., Naik, V., Stevenson, D., Tilmes, S., Voulgarakis,
1513 A., Wild, O., and Bergmann, D.: Pre-industrial to end 21st century projections of tropospheric ozone
1514 from the Atmospheric Chemistry and Climate Model Intercomparison Project (ACCMIP),
1515 *Atmospheric Chemistry and Physics*, 13, 2063-2090, 2013.
1516 Zaehle, S.: Terrestrial nitrogen–carbon cycle interactions at the global scale, *Philosophical*
1517 *Transactions of the Royal Society B: Biological Sciences*, 368, 20130125, 10.1098/rstb.2013.0125,
1518 2013.
1519 Zak, D. R., Pregitzer, K. S., Kubiske, M. E., and Burton, A. J.: Forest productivity under elevated CO₂
1520 and O₃: positive feedbacks to soil N cycling sustain decade-long net primary productivity
1521 enhancement by CO₂, *Ecology Letters*, 14, 1220-1226, 10.1111/j.1461-0248.2011.01692.x, 2011.
1522
1523
1524
1525
1526
1527
1528
1529